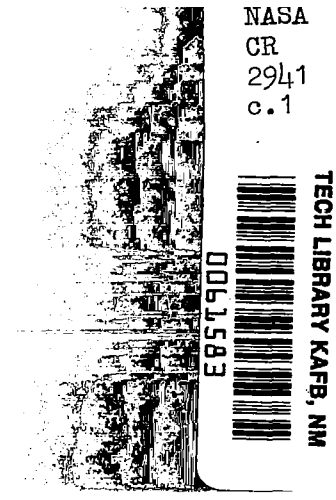

NASA Contractor Report 2941

Perturbation Solutions for Transonic Flow on the Blade-to-Blade Surface of Compressor Blade Rows

Stephen S. Stahara, Denny S. Chaussee,
and John R. Spreiter

CONTRACT NAS3-19738
JANUARY 1978

NASA

NASA Contractor Report 2941

Perturbation Solutions for Transonic Flow on the Blade-to-Blade Surface of Compressor Blade Rows

Stephen S. Stahara, Denny S. Chaussee, and John R. Spreiter
Nielsen Engineering & Research, Inc.
Mountain View, California

Prepared for
Lewis Research Center
under Contract NAS3-19738

NASA
National Aeronautics
and Space Administration

Scientific and Technical Information Office

1978

TABLE OF CONTENTS

LIST OF FIGURES

LIST OF FIGURES (CONCLUDED)

PERTURBATION SOLUTIONS FOR TRANSONIC FLOW ON THE BLADE-TO-BLADE SURFACE OF COMPRESSOR BLADE ROWS

by Stephen S. Stahara, Denny S. Chaussee, and John R. Spreiter*
Nielsen Engineering & Research, Inc.

SUMMARY

A preliminary investigation was conducted to establish the theoretical basis of perturbation techniques, with the objective of minimizing computational requirements associated with parametric studies of transonic flows in turbomachines. The theoretical analysis involved the development of perturbation methods for determining first-order changes in the flow solution due to variations of one or more geometrical or flow parameters. The formulation is primarily directed toward transonic flows on the blade-to-blade surface of a single blade-row compressor.

Two different perturbation approaches were identified and studied. They are the linear perturbation equation method and the nonlinear differencing perturbation method, and applications and results of these methods for various perturbations are presented for selected two-dimensional transonic cascade flows. The solutions obtained with the linear perturbation equation method generally indicate that good results can be anticipated for blade geometry perturbations, while less satisfactory results occur for perturbation changes in overall quantities, such as blade spacing and free-stream Mach number. These results illustrate the primary limitation of the linear perturbation equation method; that is, the basic linear variation assumption fundamental to the technique is severely restrictive for sensitive near-critical, confined transonic flows.

For flows with shock waves, it was found that a supplemental perturbation condition is necessary to account for shock displacement. Initial results obtained with the nonlinear differencing method for a supercritical cascade flow, accounting for shock displacement, display excellent agreement with corresponding nonlinear calculations.

---

*Stanford University, Dept. of Applied Mechanics, Stanford, CA.

1. INTRODUCTION

In view of the growing capability (e.g., refs. 1-4) of sophisticated numerical techniques for the calculation of transonic flows in turbomachinery--a capability certain to improve in the future--it has become apparent that a need exists for methods capable of alleviating the limitations imposed on these codes by their expensive run times. This need becomes particularly obvious and impelling when large numbers of cases are required as when examining alternative configurations in a preliminary design study or when the aerodynamic characteristics of a completed design must be determined for a wide variety of operating conditions. While direct acceleration techniques, as those developed for relaxation solutions employing nonlinear sequence transformations (ref. 5), grid refinement (ref. 6), or a multilevel grid method (ref. 7), or more efficient algorithm procedures, such as implicit rather than explicit methods (refs. 8-10) for time-marching solutions, do reduce time requirements for particular applications, they represent only a partial answer. What is ultimately needed are techniques to supplement these evolving methods which would minimize the actual number of separate solutions required in a particular application. This would be accomplished by extending, over some parametric range, the usefulness of each individual solution calculated by the more expensive base procedures.

Consequently, the basic motivation underlying this study is to extend the usefulness of such numerical solutions computed for specific turbomachinery configurations and flow conditions with a view toward reducing the computational requirements now necssary. The nature of the present investigation is exploratory in the sense that selected aspects of the procedure will be investigated, including validity, range of application, and economy. Since the basic problem selected for study, as detailed in section 2, encompasses a wide variety of parameters which can be perturbed, as well as a complete range of operating conditions, only certain selected perturbation problems will be examined in detail. The primary goal of this study is the examination and preliminary development of perturbation methods to determine first-order changes in the flow field due to variations in one or more geometrical or flow field parameters in the transonic flow on the blade-to-blade surface of a single row compressor rotor. The utlimate goal is to develop a combination of analytical perturbation procedures and associated computer codes that would minimize the amount and maximize the quality of predictive calculations needed for enconomic analysis and design study of transonic flows in turbomachinery.

2. ANALYSIS

2.1 General Procedure

The model problem chosen to test the perturbation concept has as its basis the formulation of Wu (ref. 11) used for approximating the three-dimensional flow through turbomachinery stages. That formulation reduces to a pair of two-dimensional problems that are ultimately intended to be interacted to obtain a complete solution. The essential ideas of the decomposition and of the coordinate systems used are indicated in figure 1. The hub-to-casing analysis, indicated in the figure on the left, accounts for effects of blockage of the flow area by the blades as well as the geometry of the hub and casing, but not for any circumferential variations of the flow. It provides flow properties in a meridional plane as averaged from one blade to the next, as well as the coordinates $R = R(m)$ of the curved axisymmetric stream surface upon which the blade-to-blade analysis is carried out, and the spacing $b(m)$ between two arbitrarily selected adjacent stream surfaces.

The problem of primary interest in this study is associated with the blade-to-blade surface. That problem represents the two-dimensional flow past a series of blades in the curvilinear coordinate system (m,θ) indicated on the right of figure 1 with the radius, $R(m)$, and thickness, $b(m)$, of the stream sheet provided by the previous solution of the hub-to-casing problem. Because of the more complex geometries and range of flow conditions involved, the blade-to-blade problem is the more difficult to solve. However, it is rich in variety of parameters which can be varied so that it provides an ideal test of the proposed perturbation technique. Consequently, the purpose of this study is to develop perturbation procedures which would account for first-order variations in the various geometrical quantities, flow parameters and operating conditions for the solution on the blade-to-blade surface of a single stage compressor rotor operating at transonic speeds. Possible perturbations include:

Geometrical

- Maximum thickness ratio - τ
- Thickness distribution - $\bar{f}(x)$
- Maximum camber ratio - h
- Camber distribution - $\bar{g}(x)$
- Blade spacing ratio - t/c
- Blade setting or stagger angle - λ
- Leading- and trailing-edge radii - r_{le}, r_{te}
- Channel radius distribution - $R(x)$
- Channel thickness distribution - $b(x)$

Flow

- Inlet Mach number - M_1
- Inflow angle - β_1
- Outflow angle - β_2
- Rotational speed - Ω

Operating Conditions

- Pressure ratio
- Total pressure
- Total temperature

Although ultimately a general procedure capable of treating each of these perturbations is necessary, initially we will examine, under various approximations, selected numbers of these in detail to ascertain typical behavior. Finally, we note that under certain flow conditions, such as choking, it is not possible to vary some of the parameters independently of others. This must be recognized and properly accounted for in determining the perturbation solutions.

2.2 Governing Equations

The level of approximation chosen as the starting point for analysis of the model problem is the quasi- three-dimensional Euler equations written for the curved axisymmetric blade-to-blade stream surface depicted in detail in figure 2. Applied to the rotating curvilinear coordinate system (m,θ) fixed to the blades, as indicated in that figure, the equations to be solved are:

$$\left.\begin{aligned}
&\frac{\partial \rho}{\partial t} + \frac{\partial(\rho V)}{R\partial\theta} + \frac{\partial(\rho U)}{\partial m} = -\frac{\rho U}{Rb}\frac{d(Rb)}{dm} \\
&\frac{\partial(\rho V)}{\partial t} + \frac{\partial(p + \rho V^2)}{R\partial\theta} + \frac{\partial(\rho UV)}{\partial m} = -\frac{\rho UV}{Rb}\frac{d(Rb)}{dm} - \frac{\rho U}{R}(V + 2\Omega R)\frac{dR}{dm} \\
&\frac{\partial(\rho U)}{\partial t} + \frac{\partial(\rho UV)}{R\partial\theta} + \frac{\partial(p + \rho U^2)}{\partial m} = -\frac{\rho U^2}{Rb}\frac{d(Rb)}{dm} + \frac{\rho(V + \Omega R)^2}{R}\frac{dR}{dm} \\
&\frac{\partial(\rho E_r)}{\partial t} + \frac{\partial(\rho VH_r)}{R\partial\theta} + \frac{\partial(\rho UH_r)}{\partial m} = -\frac{\rho UH_r}{Rb}\frac{d(Rb)}{dm}
\end{aligned}\right\} \quad (1)$$

Here, U and V represent the relative velocity components in the m and θ directions. The relative total energy and relative total enthalpy (rothalpy) are defined by

$$E_r = E - V\Omega R \ , \qquad H_r = H - V\Omega R \qquad (2)$$

These equations agree with those in ref. (12), and are incorporated in a computer program B2DATL (ref. 13) for transonic blade-to-blade analysis in turbomachinery. The right-hand-side terms in equations (1) arise from streamwise variation of radius $R(m)$ and thickness $b(m)$ of the stream sheet and are provided by a known hub-to-casing solution. They vanish if the equations are applied to a two-dimensional cascade flow. The corresponding equations for a non-rotating inertial system may be obtained by setting Ω to zero.

The boundary conditions corresponding to these differential equations are indicated in figure 3 for a typical single blade passage. These involve a uniform inlet condition at the upstream boundary, periodic conditions on flow quantities on the horizontal boundaries extending upstream and downstream from the leading and trailing edges of the blades, a zero normal velocity condition at the blade upper and lower surfaces, shock conditions satisfying the Rankine-Hugoniot relations at the embedded shock waves, and a uniform back pressure specification at the downstream boundary of the passage. In addition, a Kutta condition is imposed at the trailing edge, and conditions insuring the continuity of pressure and normal velocity are required along the slipstream emanating from the blade trailing edge. Location of the slipstream is initially unknown and must be found as part of the solution.

While only a few results obtained by solving these equations have been reported (refs. 2, 12), and they should be considered as provisional in view of the relative coarseness of the finite-difference calculation, those developments nevertheless indicate a powerful emerging general capability for analyzing high-speed turbomachinery. Consequently, selection of this level of solution as the starting point of the perturbation analysis provides a meaningful choice in terms of furnishing a significant goal. In addition, it provides as well an important series of simpler subcases of the general problem to check the efficiency and relative worth of the technique at various levels of accuracy.

2.3 Perturbation Concept and Methods

The basic concept underlying the present procedure is that a range of solutions in the vicinity of a previously determined or base solution can be calculated to first-order accuracy in the incremental change of the varied parameter by determining a linearized unit perturbation solution Q_p defined according to the relation

$$\underbrace{Q}_{\substack{\text{Approximate solution for conditions differing from those of the base solution by an amount characterized by } \Delta}} = \underbrace{Q_o}_{\substack{\text{Base solution for some flow quantity } Q}} + \underbrace{\Delta \cdot \{Q_p\}}_{\substack{\text{Linearized perturbation solution for a unit change of } \Delta}} \qquad (3)$$

Of primary importance is the fact that the relationship defined by equation (3) remains valid over a range of Δ, while the linearized unit perturbation solution Q_p needs to be determined only once. This, of course, provides the basis of the effectiveness of the method. The significance of the quantity Q_p is immediately recognized from the Taylor-series nature of equation (3) as the rate of change of the base flow solution Q_o with respect to the particular quantity, say q, perturbed; that is, $Q_p = (\partial Q/\partial q)_o$.

With regard to determining Q_p, two important alternative techniques are available. We refer to these as the linear perturbation equation method and the nonlinear differencing perturbation method. Although the primary emphasis of this initial study was on the linear perturbation equation method, we have in fact also employed the nonlinear differencing perturbation method. While all of these applications are discussed in detail in section 3, it is important to recognize at this point that the two methods differ in philosophy and that each has its own particular strengths and weaknesses.

2.3.1 Linear perturbation equation method.- The linear perturbation equation method represents the classical approach for performing a perturbation analysis. An overview of some of the fluid dynamic problems analyzed with this technique is given in reference 14. As the name implies, the method proceeds by establishing and solving a linear equation for the perturbation. Although in the present application our interest is confined solely to the first-order term, the complete procedure is embedded in a rational approximation scheme capable of continuation to any order. The method proceeds by expanding the dependent variables in an ascending power series of the incremental change Δ in the varied parameter, inserting that representation into the full governing equations, and then assembling the result into a corresponding series of linear equations in ascending orders of Δ. Higher-order solutions in general depend on both the base flow plus the lower-order solutions. Determination of the appropriate boundary conditions is done in a similar fashion.

The power of the linear perturbation equation method is that it requires the calculation of only one nonlinear base solution. With that information in hand, any number of individual perturbations can then be calculated, subject to the particular governing linear partial differential equation and boundary conditions which apply. The disadvantages of this method are that each perturbation problem must be posed individually, including differential equation and boundary conditions. Furthermore, the governing differential equations and boundary conditions for the perturbations must usually be approximated in order to simplify them to a point where they can be solved rapidly relative to rerunning the base flow procedure. Moreover, the perturbation solutions themselves

may be quite sensitive to the base flow solutions which always enter into the perturbation problem through the differential equation and sometimes through the boundary conditions as well.

The fundamental limitation of the linear perturbation equation technique is the restriction of the range over which the perturbation procedure remains valid to a linear one. Since this characteristic depends upon the local behavior of the base flow with respect to the varied parameter, no general statement regarding range of validity is possible. Typical behavior for a given class of flows must be ascertained by checks with the base flow procedure. Initially unknown at the outset of an application with this technique, then, are the accuracy requirements imposed on the base solution by the perturbation procedure and the range of parameter variation over which the linear assumption is valid.

2.3.2 Nonlinear differencing method.- The alternative method to the linear perturbation equation technique is the nonlinear differencing method. With this method, the perturbation solution per unit change of the varied parameter, Q_p, is determined by differencing two nonlinear base flow solutions removed from one another by some reasonable change of a particular flow or geometrical quantity. A unit perturbation solution is then obtained by dividing that result by the change in the perturbed quantity. Related solutions are determined by multiplying the unit perturbation solution by the desired parameter change and adding that result to the base flow solution. This simple procedure, however, only works directly for continuous (no shock) flows for which the perturbation changes do not alter the overall definition of the base flow. This would be the case for subcritical flow and for changes in free-stream conditions (M_1, β_1, etc.) where both blade and cascade geometry remain fixed. For those perturbations which change the geometry and hence the locations where flow quantities are determined (such as stagger angle, blade spacing, blade geometry), a coordinate stretching is necessary to insure that the flow regions remain compatible and that the perturbation solution is properly defined. Similarly, for discontinuous flows, where shocks are present and move under the perturbed conditions, special coordinate straining is necessary to account for that movement again in order to define properly the perturbation solution.

The attractiveness of the nonlinear differencing method is that it is not restricted to a linear variation range but rather replaces the nonlinear variation between two base flow solutions with a linear fit. Consequently, this de-emphasizes the dependence and sensitivity inherent in the linear perturbation equation method on the local rate of change of the base flow solution with respect to the varied quantity. For certain high-speed turbomachinery applications where, as indicated in the sketch below, the confined transonic flow may be highly sensitive, the linear range of parameter variation could be sufficiently small to be of

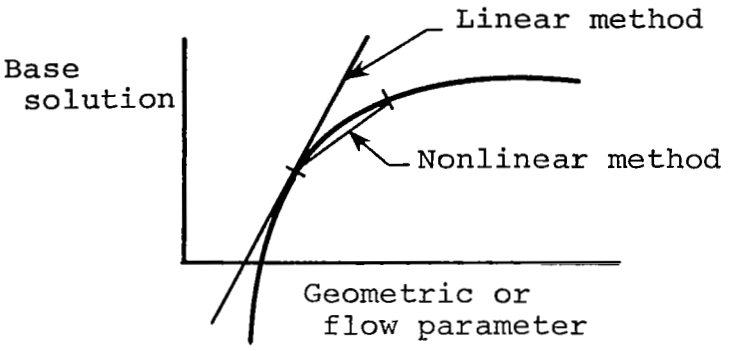

limited practical use. For those situations, the nonlinear differencing technique is more appropriate. Furthermore, other than the approximation of a linear fit between two nonlinear base solutions, the nonlinear differencing method is not restricted by further approximations with respect to the governing differential equations and boundary conditions. Rather, it retains the full character of the original methods used to calculate the base flow solutions. Moreover, no perturbation differential equations have to be solved, only algebraic ones.

The primary disadvantage of this method is that two base solutions are required for each parameter perturbation considered. For certain high-use applications, this requirement can be sufficiently disadvantageous to limit the utility of the method. For this reason, the primary emphasis of this initial study focused on the linear perturbation equation method. A description of the analysis of the linear perturbation method is provided in the following section.

2.4 Linear Perturbation Equation Method of Analysis

2.4.1 Alternate levels of approximation.- With the ultimate level of accuracy for solving the base flow set at the quasi three-dimensional Euler equations described in section 2.2, selection of the appropriate level at which to perform the perturbation analysis remains. The alternatives are:

- Quasi three-dimensional Euler equation
- Quasi three-dimensional full potential equation
- Small-disturbance transonic equation

The most obvious choice of perturbing the Euler equations is not a satisfactory one since the perturbation equations become more cumbersome than the original nonlinear equations. Furthermore,

although fast solution procedures are necessary to solve these perturbation equations, relaxation methods have not yet been fully developed (ref. 15) for such equations. Consequently, the perturbation solutions would also have to proceed by a time-marching procedure, with little chance of being significantly more economical relative to rerunning the base solution procedure again for the perturbed flow while using the original base flow as an initial guess.

An alternate choice is to select a quasi three-dimensional full potential equation approach. The significant advantages here are that of working with a single partial differential equation for the dependent variable and that relaxation methods have already proven successful for solving such problems (refs. 16 and 17). Furthermore, the method is identical in accuracy to the Euler equation approach for shockless flows and generally a very good approximation for most flows in the transonic regime where shocks are weak; that is, pre-shock Mach numbers less than 1.3. Finally, for an important series of limiting cases, checks are available with less accurate but more fully developed theories, such as transonic small-disturbance theory.

A solution procedure based on the quasi three-dimensional full potential approximation is not currently available. However, a well-documented computer code (B2DATL) based on the Euler equation formulation is available and presented in references 12 and 13. Consequently, implementation of the perturbation problem based on the full potential approach would proceed as follows.

A solution of the quasi three-dimensional Euler equations (1) and (2), as calculated by the time-marching technique described in reference 12, is assumed to represent a quasi three-dimensional full potential solution. Required potential derivatives are then determined throughout the flow by appropriate differencing of the known velocity field. Next, linear perturbation equations and boundary conditions representing various geometrical and flow perturbations about this assumed full potential base solution are derived. Finally, the perturbation equation is solved numerically using a successive line overrelaxation (SLOR) algorithm.

We note that included in this formulation is an important subset of test perturbation cases based on the small-disturbance transonic approximation. A well-tested and documented code (TSFOIL) described in reference 18 is currently available to generate appropriate small-disturbance base solutions. Although restricted in geometrical application to certain classes of two-dimensional cascades, this well-documented small-disturbance procedure can provide fast and accurate base solutions throughout the entire transonic range, including supercritical, choked, and supersonic cases useful for testing the perturbation theory.

2.4.2 Base flow boundary value problem-full potential approximation.- In this section we describe the base flow boundary value problem based on the quasi three-dimensional full potential steady approximation to the Euler equations (1) and (2). Considering the steady version of equation (1), if the θ momentum equation is multiplied by U, the m momentum equation multiplied by V, the result added, then that expression simplified by use of the continuity equation together with the isentropic relation $dp = a^2 d\rho$, the final result becomes

$$(U^2 - a^2)\frac{\partial U}{\partial m} + (V^2 - a^2)\frac{\partial V}{R\partial\theta} + VU\left(\frac{\partial U}{R\partial\theta} + \frac{\partial V}{\partial m}\right) = \frac{a^2 U}{Rb}\frac{d(Rb)}{dm} - U\Omega^2 R\frac{dR}{dm} \tag{4}$$

Furthermore, if we assumed that in the absolute (nonrotating) system that a velocity potential Φ for the complete flow exists such that

$$\begin{aligned} U &= \Phi_m \\ V &= \frac{1}{R}\Phi_\theta - \Omega R \end{aligned} \tag{5}$$

then the governing differential equation for Φ becomes

$$(\Phi_m^2 - a^2)\Phi_{mm} + [(\Phi_\theta/R - \Omega R)^2 - a^2]\Phi_{\theta\theta}/R^2 + \Phi_m(\Phi_\theta/R - \Omega R)\left(2\Phi_{m\theta}/R - \Omega\frac{dR}{dm}\right) = \frac{a^2\Phi_m}{Rb}\frac{d(Rb)}{dm} - \Phi_m\Omega^2 R\frac{dR}{dm} \tag{6}$$

where

$$a^2 = a_1^2 + \frac{1}{2}(\gamma-1)[U_1^2 + (V_1 - \Omega R)^2 - \Phi_m^2 - (\Phi_\theta/R - \Omega R)^2] \tag{7}$$

and the subscript 1 denotes uniform inlet conditions.

2.4.3 Disturbance potential boundary-value problem.- For the applications considered in this preliminary study, we are primarily concerned with nonrotating (Ω=0) cascade flows. For those situations, a convenient alternative form to equations (6) and (7) is to subtract out the incoming free-stream components from the potential and recast without approximation the governing equations in terms of a disturbance potential ϕ where

$$\Phi = Cq_1[(x\cos\beta_1 + y\sin\beta_1) + \phi] \tag{8}$$

and

$$x = m/C$$

$$y = R\theta/C$$

Here, q_1 is the free-stream velocity magnitude and β_1 the absolute angle on the stream surface of the uniform incoming flow. The governing equation for the disturbance potential ϕ follows directly by inserting equation (8) into equations (6) and (7) with $\Omega=0$. The resultant equation is given explicitly as equation (A-10) in Appendix A.

Appropriate boundary conditions for the differential equation for the disturbance potential ϕ are indicated in figure 4, where for convenience we have chosen the origin of coordinates to lie on a line halfway between the blade leading edges. We note that the primary difference between the disturbance full potential boundary condition formulation and the Euler equation formulation given in figure 3 involves conditions along the slipstream. For the disturbance potential ϕ, the conditions of continuity of pressure and normal velocity imply a jump in potential across the slipstream surface equal to the circulation around each blade. However, imposition of that potential jump along the actual location of the slipstream is unnecessary. To assure that the potential remains single-valued in the domain of interest, it is only necessary to introduce a cut along which the potential may be discontinuous and which extends from the blade surface to the downstream boundary. The location of the cut can be arbitrary and, in particular, can be chosen to lie along the horizontal boundaries extending from the trailing edges of the blades. The form of the periodic and cyclic conditions imposed at corresponding points on the upper and lower horizontal boundaries is

$$\left.\begin{aligned} &\text{Periodic:} \quad \phi_T = \phi_B \\ &\text{Cyclic:} \quad \phi_T = \phi_B + \Delta\phi_{te} \end{aligned}\right\} \tag{9}$$

where the subscripts T and B denote the top and bottom boundaries, respectively and $\Delta\phi_{te}$ is the jump in the disturbance potential at the trailing edge of the blade.

2.4.4 Perturbation disturbance potential boundary value problem.- The boundary value problems associated with perturbations about the base flow described above are established by deriving for each particular perturbation both the governing partial differential equation and associated boundary conditions. In general, both will depend on the varied parameter. The derivations are initiated on the assumption that

$$\phi = \phi^0 + \phi^1 \tag{10}$$

where ϕ^0 is the base flow disturbance potential and ϕ^1 the perturbation disturbance potential, that is, the disturbance potential associated with the parameter change away from its base value. Insertion of equation (10) into equations (6) to (8) for $\Omega=0$ leads to the following form of the governing equation for ϕ^1

$$\bar{A}\phi^1_{xx} + \bar{B}\phi^1_{xy} + \bar{C}\phi^1_{yy} + \bar{D}\phi^1_{x} + \bar{E}\phi^1_{y} = \bar{F} \tag{11}$$

where the coefficients $[\bar{A},\bar{B},\bar{C},\bar{D},\bar{E},\bar{F}]$ are in general functions of $\left[\phi^0_x,\phi^0_y,\phi^0_{xy},\phi^0_{xx},\phi^0_{yy}\right]$ and are identified in Appendix A.

2.4.5 Boundary conditions for perturbation disturbance potential.- The boundary conditions governing the various perturbations associated with equation (11) are derived in a similar fashion. The general form of the boundary conditions for an arbitrary perturbation is provided in figure 5. As anticipated, the conditions for ϕ^1 are more complex than the corresponding ones for the base flow disturbance potential ϕ^0. Based on the disturbance full potential formulation, the appropriate perturbation boundary conditions have been derived for a number of important parametric variations and are provided in Appendix B.

It is of interest to demonstrate the general procedure followed in determining boundary conditions for a typical perturbation. The basic coordinate system used is indicated in the sketch below.

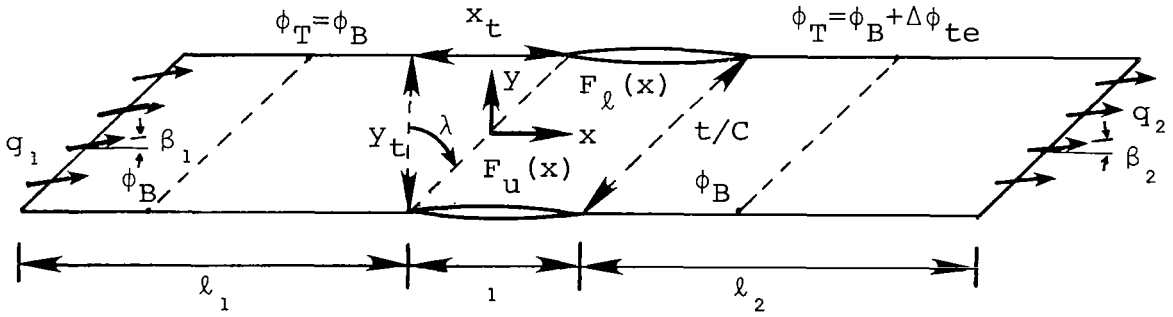

In this figure, $F_u(x)$, $F_\ell(x)$ denote the ordinates of the blade upper and lower surface, respectively, nondimensionalized by C, t/C is the blade spacing ratio, λ the stagger angle, (x_t,y_t) are given by

$$\left.\begin{aligned} x_t &= \frac{t}{C}\sin\lambda \\ y_t &= \frac{t}{C}\cos\lambda \end{aligned}\right\} \tag{12}$$

and (q_1,β_1), (q_2,β_2) are the inflow and outflow velocity and absolute flow direction. A perturbation in the stagger angle λ is considered. The boundary conditions for the blade surfaces, and the periodic and cyclic conditions are determined as follows.

(1) Blade boundary conditions: The basic tangency condions on the upper and lower surfaces of the blade are given in terms of the full potential Φ by the expressions

$$\left.\begin{aligned} \Phi_y\left(x + \frac{x_t}{2}, \frac{y_t}{2}\right) &= F'_\ell(x)\,\Phi_x\left(x + \frac{x_t}{2}, + \frac{y_t}{2}\right) \\ \Phi_y\left(x - \frac{x_t}{2}, -\frac{y_t}{2}\right) &= F'_u(x)\,\Phi_x\left(x - \frac{x_t}{2}, - \frac{y_t}{2}\right) \end{aligned}\right\} \quad 0 \le x \le 1 \tag{13}$$

The corresponding relations for the disturbance full potential ϕ are

$$\left.\begin{aligned} \Phi_y\left(x + \frac{x_t}{2}, \frac{y_t}{2}\right) &= F'_\ell(x)\cos\beta_1 - \sin\beta_1 \\ \Phi_y\left(x - \frac{x_t}{2}, -\frac{y_t}{2}\right) &= F'_u(x)\cos\beta_1 - \sin\beta_1 \end{aligned}\right\} \tag{14}$$

Considering a perturbation in stagger angle, we allow

$$\lambda = \lambda^0 + \Delta\lambda \tag{15}$$

so that

$$\left.\begin{aligned} x_t &= t\sin\lambda^0 + t\cos\lambda^0\Delta\lambda + \cdots = x_t^0 + \Delta x_t \\ y_t &= t\cos\lambda^0 - t\sin\lambda^0\Delta\lambda + \cdots = y_t^0 + \Delta y_t \end{aligned}\right\} \tag{16}$$

then,

$$\phi_y\left(x + \frac{x_t}{2}, \frac{y_t}{2}\right) = \phi_y\left(x + \frac{x_t^0}{2} + \frac{\Delta x_t}{2}, \frac{y_t^0}{2} + \frac{\Delta y_t}{2}\right) \tag{17}$$

Expanding this result about the base positions, denoted by $(\ )^0$, using a Taylor-series, we have

$$\phi_y\left(x + \frac{x_t}{2},\ \frac{y_t}{2}\right) = \phi_y\left(x + \frac{x_t^0}{2},\ \frac{y_t^0}{2}\right) + \frac{\partial}{\partial\xi}\left[\phi_y(\xi,\eta)\right]^0\left(\frac{\Delta x_t}{2}\right) + \frac{\partial}{\partial\eta}\left[\phi_y(\xi,\eta)\right]^0\left(\frac{\Delta y_t}{2}\right) + O\left(\Delta x_t^2,\ \Delta y_t^2\right) \tag{18}$$

This leads to the result that

$$\phi_y\left(x + \frac{x_t}{2},\ \frac{y_t}{2}\right) = \phi_y\left(x + \frac{x_t^0}{2},\ \frac{y_t^0}{2}\right) + \frac{t}{2C}\left[-\cos\lambda^0\phi^0_{xy}\left(x + \frac{x_t^0}{2},\ \frac{y_t^0}{2}\right) + \sin\lambda^0\phi^0_{yy}\left(x + \frac{x_t^0}{2},\ \frac{y_t^0}{2}\right)\right]\Delta\lambda + O(\Delta\lambda^2) \tag{19}$$

Introducing the following expansion

$$\phi = \phi^0 + \phi^1 \tag{20}$$

for the potential into equation (19) and ordering the results according to powers of $\Delta\lambda$, we obtain the final form of the blade upper surface boundary conditions for the base flow disturbance potential ϕ^0 and perturbation disturbance potential ϕ^1

$$\left.\begin{aligned} \phi^0_y\left(x + \frac{x_t^0}{2},\ \frac{y_t^0}{2}\right) &= F'_\ell(x)\cos\beta_1 - \sin\beta_1 \\ \phi^1_y\left(x + \frac{x_t^0}{2},\ \frac{y_t^0}{2}\right) &= \left[-\cos\lambda^0\phi^0_{xy}\left(x + \frac{x_t^0}{2},\ \frac{y_t^0}{2}\right) + \sin\lambda^0\phi^0_{yy}\left(x + \frac{x_t^0}{2},\ \frac{y_t^0}{2}\right)\right]\frac{t}{2C}\,\Delta\lambda \end{aligned}\right\} \tag{21}$$

Similarly, for the lower blade we obtain the result

$$\phi_y^0\left(x - \frac{x_t^0}{2}, - \frac{y_t^0}{2}\right) = F_u'(x)\cos\beta_1 - \sin\beta_1$$

$$\phi_y^1\left(x - \frac{x_t^0}{2}, - \frac{y_t^0}{2}\right) = \left[\cos\lambda^0\phi_{xy}^0\left(x - \frac{x_t^0}{2}, - \frac{y_t^0}{2}\right) - \sin\lambda^0\phi_{yy}^0\left(x - \frac{x_t^0}{2}, - \frac{y_t^0}{2}\right)\right]\frac{t}{2C}\Delta\lambda \tag{22}$$

(2) Periodic condition: The basic periodic condition, equation (9), is given by the statement

$$\phi\left(x + \frac{x_t}{2}, \frac{y_t}{2}\right) = \phi\left(x - \frac{x_t}{2}, - \frac{y_t}{2}\right) \qquad -\ell_1 < x < 0 \tag{23}$$

As before, by using the expansions in equations (16) and (20), Taylor-series expanding about the base flow values, and then ordering that result according to powers of $\Delta\lambda$, we obtain the following forms of the periodic conditions for the base flow and perturbation component

$$\left.\begin{aligned}\phi^0\left(x + \frac{x_t^0}{2}, \frac{y_t^0}{2}\right) &= \phi^0\left(x - \frac{x_t^0}{2}, - \frac{y_t^0}{2}\right)\\ \phi^1\left(x + \frac{x_t^0}{2}, \frac{y_t^0}{2}\right) &= \phi^1\left(x - \frac{x_t^0}{2}, - \frac{y_t^0}{2}\right) + \left[-\cos\lambda^0\phi_x^0\left(x - \frac{x_t^0}{2}, - \frac{y_t^0}{2}\right) + \sin\lambda^0\phi_y^0\left(x - \frac{x_t^0}{2}, - \frac{y_t^0}{2}\right)\right]\frac{t}{2C}\Delta\lambda\\ &\qquad -\ell_1 < x < 0\end{aligned}\right\} \tag{24}$$

where the periodic condition on the base flow velocity components

$$\left.\begin{aligned}\phi_x^0\left(x + \frac{x_t^0}{2}, \frac{y_t^0}{2}\right) &= \phi_x^0\left(x - \frac{x_t^0}{2}, - \frac{y_t^0}{2}\right)\\ \phi_y^0\left(x + \frac{x_t^0}{2}, \frac{y_t^0}{2}\right) &= \phi_y^0\left(x - \frac{x_t^0}{2}, - \frac{y_t^0}{2}\right)\end{aligned}\right\} \tag{25}$$

has also been employed.

(3) Cyclic boundary condition: The cyclic boundary condition, equation (9), which accounts for the jump in potential across the passage due to circulation is given by

$$\phi\left(x + \frac{x_t}{2}, \frac{y_t}{2}\right) = \phi\left(x - \frac{x_t}{2}, -\frac{y_t}{2}\right) + \Delta\phi_{te} \qquad 1 < x < 1 + \ell_2 \tag{26}$$

where

$$\Delta\phi_{te} = \phi\left(1 + \frac{x_t}{2}, \frac{y_t}{2}\right) - \phi\left(1 - \frac{x_t}{2}, -\frac{y_t}{2}\right) \tag{27}$$

In addition to the same changes associated with the periodic condition, the cyclic condition involves changes in $\Delta\phi_{te}$ as well which must be considered. Application of the same expansion procedure to equation (27) leads to the result that

$$\Delta\phi_{te} = \Delta\phi^0_{te} + \left\{\Delta\phi^1_{te} + \left[\cos\lambda^0\phi^0_x\left(1 - \frac{x^0_t}{2}, -\frac{y^0_t}{2}\right) - \sin\lambda^0\phi^0_y\left(1 - \frac{x^0_t}{2}, -\frac{y^0_t}{2}\right)\right]\frac{t}{C}\,\Delta\lambda\right\} \tag{28}$$

where

$$\left.\begin{aligned}\Delta\phi^0_{te} &= \phi^0\left(1 + \frac{x^0_t}{2}, \frac{y^0_t}{2}\right) - \phi^0\left(1 - \frac{x^0_t}{2}, -\frac{y^0_t}{2}\right)\\ \Delta\phi^1_{te} &= \phi^1\left(1 + \frac{x^0_t}{2}, \frac{y^0_t}{2}\right) - \phi^1\left(1 - \frac{x^0_t}{2}, -\frac{y^0_t}{2}\right)\end{aligned}\right\} \tag{29}$$

Thus, the final form of the cyclic boundary conditions is

$$\left.\begin{aligned}\phi^0\left(x + \frac{x^0_t}{2}, \frac{y^0_t}{2}\right) &= \phi^0\left(x - \frac{x^0_t}{2}, -\frac{y^0_t}{2}\right) + \Delta\phi^0_{te}\\ \phi^1\left(x + \frac{x^0_t}{2}, \frac{y^0_t}{2}\right) &= \phi^1\left(x - \frac{x^0_t}{2}, -\frac{y^0_t}{2}\right) + \Delta\phi^1_{te}\\ &\quad + \cos\lambda^0\left[\phi^0_x\left(1 - \frac{x^0_t}{2}, -\frac{y^0_t}{2}\right) - \phi^0_x\left(x - \frac{x^0_t}{2}, -\frac{y^0_t}{2}\right)\right]\frac{t}{C}\,\Delta\lambda\\ &\quad - \sin\lambda^0\left[\phi^0_y\left(1 - \frac{x^0_t}{2}, -\frac{y^0_t}{2}\right) - \phi^0_y\left(x - \frac{x^0_t}{2}, -\frac{y^0_t}{2}\right)\right]\frac{t}{C}\,\Delta\lambda\end{aligned}\right\} \tag{30}$$

$$1 < x < 1 + \ell_2$$

As mentioned previously, corresponding results for a number of important perturbations have been derived and are provided in Appendix B.

2.4.6 Transonic small-disturbance formulation.- Finally, we note that a variety of subcases are contained within the full potential approximation described above for the base flow (eqs. (6) to (8)) and for the perturbation component (eq. (11)) and their associated boundary conditions. These include two-dimensional cascade flows and two-dimensional small-disturbance cascade flows. In view of the importance of the two-dimensional small-disturbance approximation to this initial study, we outline briefly here the simplification of the full potential formulation to the small-disturbance level.

By considering the two-dimensional [(db/dx) = (dR/dx) = 0] nonrotating ($\Omega = 0$) form of equations (6) to (8), and introducing the scaling parameters

$$\tilde{y} = \tau^{1/3} M_1^{2/3} y \tag{31}$$

$$\Phi = Cq_1 \left\{ x + \frac{\tau^{2/3}}{M_1^{2/3}} \tilde{\phi}(x,\tilde{y}) \right\} \tag{32}$$

appropriate to small-disturbance flows into those equations, the following differential equation in conservation form results for the transonic small-disturbance velocity potential $\tilde{\phi}$:

$$\left[K\tilde{\phi}_x - \left(\frac{\gamma+1}{2} \right) \tilde{\phi}_x^2 \right]_x + \left[\tilde{\phi}_{\tilde{y}} \right]_{\tilde{y}} = 0 \tag{33}$$

where

$$K = \frac{1 - M_1^2}{\tau^{2/3} M_1^{4/3}} \tag{34}$$

The corresponding differential equation for the perturbation transonic small-disturbance potential $\tilde{\phi}^1$ defined according to

$$\tilde{\phi} = \tilde{\phi}^0 + \tilde{\phi}^1 \tag{35}$$

is given in conservation form by

$$\left[\left(K - (\gamma+1)\tilde{\phi}_x^0\right)\tilde{\phi}_x^1\right]_x + \left[\tilde{\phi}_{\tilde{y}}\right]_{\tilde{y}} = 0 \qquad (36)$$

2.5 Base Flow Solution Procedures

In order to determine the base flows about which perturbations are to be considered, two solution procedures were employed. These are (1) the quasi three-dimensional Euler equation solver B2DATL developed in references 12 and 13 which solves equations (1) subject to the boundary conditions depicted in figure 3, and (2) the two-dimensional small-disturbance transonic equation solver TSFOIL developed in reference 18 which solves equation (33) subject to boundary conditions appropriate to an unstaggered nonlifting cascade. While the B2DATL code provides the ultimate general capability for determining base flow solutions for the present perturbation study, run time and core storage requirements of that procedure limited the variety of perturbation applications which could be investigated. Notwithstanding the limitations of zero stagger, camber, and lift for cascade applications of the TSFOIL code, that procedure provides fast and accurate base solutions throughout the entire transonic range, including supercritical, choked, and supersonic flows. Figures 6 through 8 demonstrate the validity of that procedure to provide reliable base flow cascade solutions. Figure 6 displays results for the surface pressures predicted by TSFOIL for purely subsonic flow past two unstaggered nonlifting cascades with different pitch-to-chord ratios H/C and having biconvex blade profiles for several different thickness ratios. The plot on the left displays results for $H/C = 0.75$. The dashed line indicates the result of linear theory for $\tau = 0.06$ and provides some idea of the magnitude of the nonlinear effects present even at this low a Mach number. The analogous results in the plot on the right for $H/C = 2.0$ indicate less severe but still appreciable nonlinear effects for this less confined flow. Both of these results display the need for a nonlinear calculation. Figure 7 exhibits the location of the sonic line and shock waves during the onset of choked flow as predicted by TSFOIL for a cascade of unstaggered, nonlifting parabolic-arc blade profiles with $\tau = 0.07$ and $H/C = 2.0$. We note the small Mach number range between the onset of supercritical flow and choking, and the movement of the shock wave downstream after choking has occurred with decreasing downstream pressure. Figure 8 exhibits the pressure distribution on the cascade centerline between the two blades. These results verify those measured and predicted for choked flow by Collins and Krupp (ref. 19). Finally, figure 9 displays the sensitivity of surface pressure distributions to thickness ratio for this cascade for $M = 0.80$ as the thickness ratio varies from $\tau = 0.065$ to 0.075, and indicates again the high sensitivity of confined transonic flows.

3. RESULTS

3.1 Linear Perturbation Equation Method

Theoretical results obtained from the linear perturbation equation method for various parameter perturbations are provided in figures 10 through 18. Initially presented are results based on the small-disturbance transonic equation formulation given in equations (31) to (36). Those results extend through the transonic regime and include subcritical, supercritical, and supersonic flow situations. Also presented are subcritical perturbation results obtained using Euler equation base solutions.

In figure 10, comparisons are displayed for perturbation solutions associated with thickness ratio changes of two unstaggered nonlifting cascades composed of biconvex profiles in a subcritical flow with free-stream Mach number $M_1 = 0.60$. The plot on the left exhibits the comparisons for a pitch-to-chord ratio $H/C = 0.75$.

The solid lines indicate the results obtained by using the base solution procedure (TSFOIL) for the three thickness ratios shown. The two solid line results for thickness ratios τ equal to 0.06 and 0.08 are meant to be compared with those indicated by the dashed lines. The dashed results were obtained using the perturbation method based on solving equation (36) with an SLOR relaxation algorithm (CASCDE) subject to the boundary conditions for a thickness ratio perturbation given in Appendix B. The base flow solution for thickness ratio equal to 0.07 was used to evaluate the coefficients in equation (36). The results with $\Delta\tau = \pm 0.01$ were then added to the $\tau = 0.07$ base flow.

The good agreement between the perturbation and base flow results is impressive considering that at this spacing the flow is relatively sensitive to changes in geometry. Numerical experiments show that this flow chokes at M_1 just under 0.7. Furthermore, the change in thickness ratio considered here of 1 in 7 is 14 percent, which is not a small perturbation. Analogous results are presented in the plot on the right for $H/C = 2.0$. In this case, where the flow is less confined, the perturbation results are essentially identical with those predicted by using the base flow method.

In figure 11, subcritical results are given for perturbation solutions associated with a change in pitch-to-chord ratio H/C of an unstaggered nonlifting cascade. This perturbation is fundamentally different from that associated with a $\Delta\tau$ perturbation in its dependence on boundary data. As indicated in Appendix B and repeated in the sketch below, the primary characteristic of this perturbation is that the boundary conditions

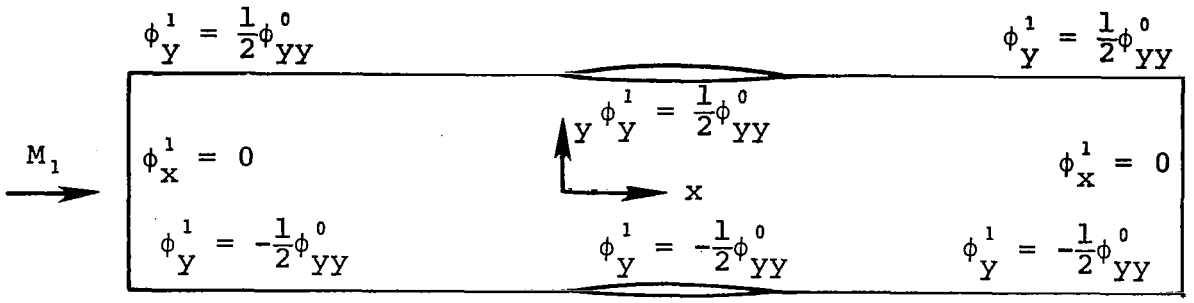

involve the second derivative of the base flow potential along the dividing streamline and blade surface. Because of this, this particular perturbation problem provides a good test of the sensitivity of the perturbation procedure to boundary data involving base flow quantities.

In figure 11, the dashed lines indicate the perturbation predicted results for $\Delta H/C = \pm 0.10$. These were obtained by solving the perturbation equation (36) subject to the boundary conditions indicated above, and then adding those results to the $H/C = 0.75$ base flow solution. Comparisons with the corresponding nonlinear TSFOIL solutions for $H/C = 0.65$ and 0.85 indicate reasonably good agreement for the perturbation change to a higher spacing ($H/C = 0.75$ to 0.85), and somewhat less satisfactory agreement for the change to a closer spacing ($H/C = 0.75$ to 0.65). However, the nonlinear TSFOIL results indicate a negative peak pressure coefficient change approximately 50 percent larger for the $H/C = 0.75$ to 0.65 change than for the $H/C = 0.75$ to 0.85 change. This clearly demonstrates the strong nonlinearity of the flow as the spacing is decreased. Furthermore, the nonlinearity is such that a $\Delta H/C$ decrease of 0.10 from the base flow at $H/C = 0.75$ is far beyond a linear change, while a corresponding increase is significantly closer to linear.

A satisfying feature of the accuracy of these results is that, for a $\Delta H/C$ perturbation, the perturbation pressure coefficients are composed of two terms; that is,

$$C_{p_u}^1(x,0) = -2\frac{\Delta H}{C}\left[\phi_x^1(x,0) + F_u''(x)\right]$$

with an analogous result for $C_{p_\ell}^1(x,H)$. For the results plotted in figure 11, $F_u''(x) = -4\tau = -0.28$. Consequently, the perturbation pressure coefficient is the difference of two large quantities, so that the accuracy in the comparisons with the nonlinear TSFOIL results is even more impressive.

Finally, we note that preliminary calculations of this perturbation problem indicated a strong sensitivity to the accuracy of the ϕ_{yy}^0 distribution employed in the boundary data. It was found that grid clustering in the y direction near the boundaries was essential in order to obtain accurate perturbation

results. This, of course, necessitated a somewhat finer grid and more accurately defined base flow than would normally have been used.

In figure 12, the final subcritical results based on TSFOIL base solutions are presented for a perturbation in oncoming Mach number. In this instance, the boundary conditions for the perturbation are all homogeneous, but the governing equation (Appendix A) contains forcing terms on the right-hand side involving base flow quantities. We note that the perturbation problems involving changes in stream sheet thickness b and radial divergence R, which have not yet been considered, involve the same basic problem formulation as this ΔM_1 perturbation; that is, homogeneous boundary data together with a governing differential equation having forcing terms on the right-hand side.

With regard to the comparisons shown in figure 12, we note an extremely strong nonlinearity of the flow as the Mach number is increased. In particular, the nonlinear TSFOIL solutions show that the negative peak pressure coefficient change from $M_1 = 0.60$ to 0.50 is approximately 20 percent less than the $M_1 = 0.60$ to 0.65 change, which indicates a 120 percent difference per unit M_1 change between increasing and decreasing M_1. Consequently, while the linear perturbation prediction falls somewhat short in predicting the M_1 decrease, the behavior for an M_1 increase is so strongly nonlinear that the linear method does not apply over a $\Delta M_1 = 0.05$ range.

In all of the subcritical perturbation results provided in figures 10 through 12, the stability and convergence properties of the CASCDE solutions were excellent. No problems were encountered and convergence was usually obtained within 200-300 SLOR iterations on a fine (103×21) mesh.

Results for perturbations of supercritical cascade flows with TSFOIL base solutions are shown in figures 13 and 14. In figure 13, comparisons between the perturbation and base flow methods are given for a thickness ratio perturbation of the strongly supercritical flow past an unstaggered nonlifting cascade of parabolic-arc blade profiles with $H/C = 2.0$, $M_1 = 0.80$, and base thickness ratio $\tau = 0.075$. A perturbation solution for $\Delta\tau = 0.002$ has been added to the $\tau = 0.075$ base solution to produce the dashed line result. Comparison with the nonlinear TSFOIL result for $\tau = 0.073$ indicates that the perturbation prediction is essentially identical with the nonlinear result until the shock wave is approached, at which point a discrepancy appears. Beyond the shock, agreement again becomes good. The reason for the discrepancy near the shock is that the conservation form of the differential equation used to calculate the perturbation solution (eq. (36)) essentially satisfies the appropriate perturbation jump condition, but at the old (i.e., base

flow) location rather than new location of the shock. If the shock were somehow constrained not to move due to the flow perturbation, the present formulation would be valid. Thus, in the present formulation the proper shock condition is satisfied but at the wrong location. To remedy this, the perturbation problem must be supplemented by an additional condition at the base flow shock points which account for shock displacement. A similar condition holds true at sonic points, which are also displaced. However, since the flow is continuous at those points, the supplementary conditions there, although necessary to impose, would not be expected to have a large effect on the perturbation solution.

In figure 14, analogous results are presented for a supercritical $\Delta H/C$ perturbation. In this instance, a significant discrepancy exists in the perturbation solution in the vicinity of the shock wave, where the perturbation solution exhibits a large oscillatory behavior. The cause of this discrepancy is clearly evident in the plot on the bottom of the figure, which displays the boundary data; that is, ϕ^0_{yy} along the blade surface. Extreme irregularities in the form of strong oscillations, absent in the subcritical case, are now present and located in the vicinity of the shock wave. Application of the supplemented perturbation shock point condition, as discussed previously, would no doubt improve the above comparison. However, the irregular behavior of the boundary distribution of ϕ^0_{yy} shown above may in fact be proper in the vicinity of the shock since large accelerations would be expected to occur. Should this be the case, it would be difficult to achieve accuracy for the $\Delta H/C$ perturbation with the linear perturbation equation method for both supercritical and supersonic flows. Nevertheless, in spite of these irregularities in boundary data no convergence or stability problems were encountered in the CASCDE solutions for these flows.

In figures 15 and 16, results are presented for perturbations of supersonic cascade flows with TSFOIL base solutions. Figure 15 displays comparisons for a thickness ratio perturbation of $\Delta\tau = 0.005$ of an unstaggered nonlifting parabolic-arc profile cascade with $M_1 = 1.15$, $H/C = 2.0$, and $\tau = 0.70$. The effect of not taking proper account of shock displacement is clearly evident in this example. The displacement of the bow shock, which is generally more sensitive to movement than surface shocks, is not well accounted for within the present formulation and may be the cause of the discrepancies on the blade surface. Corresponding results shown in figure 16 for an upstream Mach number perturbation, however, display quite good agreement. Further testing would be required to determine whether this is fortuitous or whether the M_1 perturbation actually does become less sensitive and amenable to linear analysis at supersonic Mach numbers.

The final comparisons presented using the linear perturbation equation method are provided in figures 17 and 18. In these results, the base flow solutions are subcritical Euler equation solutions obtained from the B2DATL code (refs. 12,13). The cascade geometry used was identical to that employed in the TSFOIL solutions; that is, an unstaggered cascade of parabolic-arc blade profiles. In addition, in order to facilitate comparison with previous TSFOIL results, a small-disturbance perturbation formulation was used. Figure 17 displays comparisons for a thickness ratio perturbation of a nonlifting cascade with $M_1 = 0.6$, $H/C = 2.0$, and $\tau = 0.07$. We note that in spite of the irregularity in the base flow solution near the leading edge, which is apparently due to the particular treatment of the sharp leading edge, and also the erroneous asymmetry of the solution about the blade midpoint, the perturbation procedure with $\Delta\tau = \pm 0.01$ predicts excellent agreement with the base flow results at $\tau = 0.06$ and 0.08. A similar comparison is given in figure 18, which displays results for a $\Delta\tau = -0.01$ perturbation about the same base flow conditions and geometry but now including lift, with the inlet flow angle $\beta_1 = 4°$. Again, the agreement between base flow and perturbation predictions is excellent.

3.2 Nonlinear Differencing Perturbation Method

The initial impetus for application of the nonlinear differencing perturbation method was twofold: (1) to attempt to correct the previous deficiencies associated with shock displacement in the supercritical and supersonic perturbation problems discussed above, and (2) to determine whether this method would provide more satisfactory results for these more highly nonlinear flows than the linear perturbation equation method. Both of these characteristics are evident in the example selected for preliminary calculation by this method. This is the supercritical flow initially presented in figure 9 for flow past an unstaggered nonlifting cascade of parabolic-arc blades of various thickness ratios with $H/C = 2.0$ and $M_1 = 0.80$. The extreme sensitivity of the solution to small changes in thickness ratio is evident. The corresponding $\Delta\tau$ perturbation solution via the linear perturbation equation method was provided in figure 13 and displays the typical shock displacement discrepancy.

The source of difficulty as well as the remedy associated with defining a proper perturbation solution when shock waves are present and displaced by a perturbation is provided graphically by the sketches in figure 19. The sketch on the left illustrates as the shaded area the perturbation between two nonlinear supercritical solutions. We note that the perturbation is well defined and small everywhere except in the vicinity of the shock waves. In that region, due to shock movement, the perturbation becomes of the same order as the base flow solution and the entire

perturbation concept breaks down. The correction to this is indicated in the figure on the right in which coordinate straining is used to move the shock of the perturbed flow back to the base flow location. The result is that the perturbation now remains small and well defined everywhere.

Initial results obtained by using such a coordinate straining technique have been recently reported (ref. 20) for small-disturbance flows past an isolated, nonlifting symmetric airfoil in which the shock wave that appears on the airfoil surface is assumed to be normal to the flow. We have extended that result to the cascade flows shown in figure 9. The results obtained by using coordinate straining together with differencing of two nonlinear solutions are shown in figure 20. Here, the base flow solutions shown in figure 9 for $\tau = 0.075$ and 0.073 were differenced, after shock straining was employed, to define the unit perturbation solutions. Then, that perturbation solution was employed together with the base solution of $\tau = 0.073$ to predict the solutions for $\tau = 0.072$, 0.070, 0.068, and 0.065. In each of the cases shown, the perturbation results ($\odot$) are meant to be compared with the dashed (---) solutions which represent the nonlinear TSFOIL solution at the new thickness ratio. We note that in every case the agreement is outstanding, particularly in view of the large extrapolations involved. The only exceptions are several of the flagged ($\odot$) points designated on the figure as shock-capture points. Those discrepancies are not the fault of the straining procedure, but rather arise because of the shock smearing characteristic of the shock-capture procedure employed in TSFOIL. The coordinate straining procedure is derived on the basis of a sharp shock discontinuity. When shock-capture methods are employed for determining base flow solutions, the shock points will be somewhat smeared (refs. 18 and 21) as shown in figure 20. Corrections to this can be made directly by modifying the perturbation procedure in the vicinity of the shock either by smoothing or weighting the shock-capture points.

4. CONCLUSIONS AND RECOMMENDATIONS

Theoretical analysis and associated development of computational programs have been carried out in a preliminary application of perturbations methods to transonic flows in turbomachines. The theoretical analysis involved development of perturbation methods for determining first-order changes in the flow field due to variations in one or more geometrical or flow parameters for transonic flows on the blade-to-blade surface of a single blade-row compressor. The perturbation formulation is based on the quasi three-dimensional full potential approximation to the flow and is developed in a curvilinear coordinate system fixed to the blades. Included in the formulation are variations in stream sheet thickness and radius. Applications and results are presented for selected two-dimensional cascade flows.

Two different perturbation approaches were identified and studied. They are:

- Linear perturbation equation method
- Nonlinear differencing perturbation method

With regard to the linear perturbation equation method, boundary value problems associated with a variety of perturbations were developed based on the full potential formulation. These include variations in maximum blade thickness, blade spacing, inflow Mach number, inflow angle, maximum blade camber, and stagger. Also developed were the special forms of these boundary value problems based on the transonic small-disturbance formulation for maximum blade thickness, blade spacing, and inflow Mach number.

Perturbation solutions obtained with the linear perturbation equation method generally indicate that good results can be anticipated for blade geometry perturbations, such as blade thickness and angle of attack, for subcritical flows. This was found to be true both for perturbations of transonic small-disturbance flows as well as of the Euler equation flows developed in reference 12. Reasonable but less satisfactory results were obtained for perturbation changes in overall quantities, such as blade spacing and free-stream Mach number, particularly when H/C was less than 1 and the flow was supercritical. Because these perturbations alter the basic character of the flow more rapidly, it is anticipated that they will prove to be more difficult to predict satisfactorily. Those results serve to point out the primary limitation of the linear perturbation equation method; that is, for near-critical transonic flows and blade spacings typical of modern compressor blade rows, the basic linear variation assumption fundamental to the technique is severely restrictive.

For the perturbation problem associated with blade spacing changes, where the boundary conditions as well as the differential equation involve base flow quantities, a sensitivity to base solution accuracy was found. A direct remedy to this is to recast the perturbation problem in coordinates strained locally in such a fashion as to eliminate the base flow quantities from the boundary conditions. Although this procedure would complicate the perturbation differential equation somewhat, the sensitivity of the solution would be lessened and the overall perturbation solution enhanced.

Additionally, it was found that for flows with shock waves, a supplemental perturbation boundary condition is required at the shock wave. This is needed to account for shock displacement. Results obtained for supercritical and supersonic flows without this boundary condition are clearly unsatisfactory.

The stability and convergence properties, however, of the linear perturbation equation code (CASCDE) that was developed to obtain finite-difference solutions of the various perturbation problems were very good for all the perturbations examined. This included the subcritical, supercritical, and supersonic cases considered, and held true in spite of strong irregularities in the base flow solution, such as displayed in the boundary data for the supercritical spacing perturbation (fig. 14) and the strong leading-edge inaccuracies in the Euler equation solutions for thickness (fig. 17) and lift (fig. 18). Consequently, rapid and accurate converged solutions are definitely achievable with this method.

In order to examine perturbation results which account for shock displacement, preliminary application of the nonlinear differencing method with coordinate straining was made to a supercritical cascade flow. The results obtained display outstanding agreement with corresponding nonlinear calculations. Aside from some slight discrepancies associated not with the perturbation technique or the straining but rather with the shock smearing character of the base flow procedure used (TSFOIL), the method was able to predict from two strongly supercritical solutions satisfactory results all the way down to the limiting subcritical/supercritical flow.

On the basis of this preliminary study, it is evident that the two perturbation methods examined possess definite merit for application to certain transonic flow problems in turbomachines. Results obtained for selected perturbation problems indicate that these methods are capable of providing neighboring solutions of good accuracy on an economical basis. Further development is needed, however, to provide a computational tool of practical utility for a wide range of perturbations. Because each of the perturbation methods studied possesses distinct advantages, we

suggest that development of both is warranted. With regard to the linear perturbation equation method, inclusion of the shock displacement condition is needed and can be accomplished via coordinate straining. Similarly, for those perturbation problems whose boundary conditions involve base flow quantities, local coordinate straining should be used to eliminate that dependence and corresponding solution sensitivity. Finally, a variety of cases should be studied at flow conditions throughout the transonic regime to establish solution accuracy and range of validity. With regard to the nonlinear differencing method, in view of the success of this method in the initial application to a supercritical cascade flow, it appears to be an ideal technique for perturbing certain highly sensitive transonic flows. Consequently, it should be applied to a wide variety of perturbation problems and, in particular, to strongly supercritical cases. In addition, two-dimensional straining should be incorporated in order to enable prediction of flow field as well as blade surface properties.

APPENDIX A

DERIVATION OF PERTURBATION DISTURBANCE POTENTIAL EQUATIONS

This appendix outlines the derivation of and provides expressions for the coefficients $[\bar{A},\bar{B},\bar{C},\bar{D},\bar{E},\bar{F}]$ associated with the differential equation (11) governing the perturbation disturbance potential ϕ^1. The basis of the analysis is the nonrotating ($\Omega=0$) form of equation (6) given by

$$(\Phi_m^2 - a^2)\Phi_{mm} + \left[(\Phi_\theta/R)^2 - a^2\right]\Phi_{\theta\theta}/R^2 + \frac{2}{R^2}\Phi_m\Phi_\theta\Phi_{m\theta} = \frac{a^2\Phi_m}{Rb}\frac{d(Rb)}{dm} \tag{A-1}$$

where

$$a^2 = a_1^2 + \frac{1}{2}(\gamma - 1)[U_1^2 + V_1^2 - \Phi_m^2 - (\Phi_\theta/R)^2] \tag{A-2}$$

and the subscript 1 denotes uniform inlet conditions.

It is convenient to employ a disturbance potential ϕ defined according to

$$\Phi = Cq_1[x\cos\beta_1 + y\sin\beta_1 + \phi] \tag{A-3}$$

where

$$q_1 = \sqrt{U_1^2 + V_1^2} \tag{A-4}$$

$$\beta_1 = \tan^{-1}\left(\frac{V_1}{U_1}\right) \tag{A-5}$$

$$x = m/C \tag{A-6}$$

$$y = R\theta/C \tag{A-7}$$

The perturbation coefficients $[\bar{A},\bar{B},\bar{C},\bar{D},\bar{E},\bar{F}]$ are determined by first expanding the potential ϕ and the various parameters in the differential equations as follows:

$$\left.\begin{aligned} \phi &= \phi^0 + \phi^1 \\ \beta_1 &= \beta_1^0 + \Delta\beta_1 \\ M_1 &= M_1^0 + \Delta M_1 \\ \frac{Rb}{C^2} &= \frac{(Rb)^0}{C^2} + \Delta\frac{(Rb)}{C^2} \end{aligned}\right\} \qquad \text{(A-8)}$$

where M_1 is defined by

$$M_1 = \frac{q_1}{a_1} \qquad \text{(A-9)}$$

By inserting equations (A-3) through (A-9) into equations (A-1) and (A-2),expanding the result, neglecting terms of higher than first order in ϕ^1, $\Delta\beta_1$, ΔM_1, and $\Delta\frac{(Rb)}{C^2}$, and then ordering the resulting equations according to base flow $(\,)^0$ and perturbation (ϕ^1, $\Delta\beta_1$, ΔM_1, $\Delta\frac{(Rb)}{C^2}$) quantities, the following differential equations result for the potentials (ϕ^0, ϕ^1):

$$\left[\left(\cos\beta_1^0 + \phi_x^0\right)^2 - a_0^2\right]\phi_{xx}^0 + \left[\left(\sin\beta_1^0 + \phi_y^0\right)^2 - a_0^2\right]\phi_{yy}^0 + \left(\cos\beta_1^0 + \phi_x^0\right)\left(\sin\beta_1^0 + \phi_y^0\right)\phi_{xy}^0 = a_0^2\left(\cos\beta_1^0 + \phi_x^0\right)\frac{d}{dx}\ln\frac{(Rb)^0}{C^2} \qquad \text{(A-10)}$$

and

$$\bar{A}\phi_{xx}^1 + \bar{B}\phi_{xy}^1 + \bar{C}\phi_{yy}^1 + \bar{D}\phi_x^1 + \bar{E}\phi_y^1 = \bar{F} \qquad \text{(A-11)}$$

where

$$a_0^2 = \frac{a^{0\,2}}{a_1^2} = \frac{1}{(M_1^0)^2} - \frac{1}{2}(\gamma-1)\left[\left(2\cos\beta_1^0 + \phi_x^0\right)\phi_x^0 + \left(2\sin\beta_1^0 + \phi_y^0\right)\phi_y^0\right] \qquad \text{(A-12)}$$

$$\bar{A} = \left[\left(\cos \beta_1^0 + \phi_x^0\right)^2 - a_0^2\right] \tag{A-13}$$

$$\bar{B} = \left[2\left(\cos \beta_1^0 + \phi_x^0\right)\left(\sin \beta_1^0 + \phi_y^0\right)\right] \tag{A-14}$$

$$\bar{C} = \left[\left(\sin \beta_1^0 + \phi_y^0\right)^2 - a_0^2\right] \tag{A-15}$$

$$\bar{D} = \left[\left(\cos \beta_1^0 + \phi_x^0\right)\left\{(\gamma+1)\phi_{xx}^0 + (\gamma-1)\phi_{yy}^0\right\} + 2\left(\sin \beta_1^0 + \phi_y^0\right)\phi_{xy}^0 - \left\{a_0^2 - (\gamma-1)\left(\cos \beta_1^0 + \phi_x^0\right)^2\right\}\frac{d}{dx} \ln \frac{(Rb)^0}{c^2}\right] \tag{A-16}$$

$$\bar{E} = \left[\left(\sin \beta_1^0 + \phi_y^0\right)\left\{(\gamma-1)\phi_{xx}^0 + (\gamma+1)\phi_{yy}^0\right\} + 2\left(\cos \beta_1^0 + \phi_x^0\right)\phi_{xy}^0 + (\gamma-1)\left(\sin \beta_1^0 + \phi_y^0\right)\left(\cos \beta_1^0 + \phi_x^0\right)\frac{d}{dx} \ln \frac{(Rb)^0}{c^2}\right] \tag{A-17}$$

$$\begin{aligned}\bar{F} = \Bigg[&\left\{2 \sin \beta_1^0 \left(\cos \beta_1^0 + \phi_x^0\right) + (\gamma-1)\left(\sin \beta_1^0 \phi_x^0 - \cos \beta_1^0 \phi_y^0\right)\right\}\phi_{xx}^0 \\ &- \left\{2 \cos \beta_1^0 \left(\sin \beta_1^0 + \phi_y^0\right) - (\gamma-1)\left(\sin \beta_1^0 \phi_x^0 - \cos \beta_1^0 \phi_y^0\right)\right\}\phi_{xy}^0 \\ &+ \left\{2 \sin \beta_1^0 \left(\sin \beta_1^0 + \phi_y^0\right) - \cos \beta_1^0 \left(\cos \beta_1^0 + \phi_x^0\right)\right\}\phi_{xy}^0 \\ &- \Bigg\{a_0^2 \sin \beta_1^0 - (\gamma-1)\Big[\sin \beta_1^0 \phi_x^0 \\ &\qquad - \cos \beta_1^0 \phi_y^0\Big]\left(\cos \beta_1^0 + \phi_x^0\right)\Bigg\}\frac{d}{dx} \ln \frac{(Rb)^0}{c^2}\Bigg] \cdot \Delta\beta_1\end{aligned} \tag{A-18}$$

(continued on next page)

$$- \left[\frac{2}{(M_1^0)^3} \left\{ \phi_{xx}^0 + \phi_{yy}^0 + \left[\cos \beta_1^0 + \phi_x^0 \right] \frac{d}{dx} \ln \frac{(Rb)^0}{c^2} \right\} \right] \cdot \Delta M_1$$

$$+ \left[a_0^2 \left[\cos \beta_1^0 + \phi_x^0 \right] / \frac{(Rb)^0}{c^2} \right] \frac{d}{dx} \left[\Delta \frac{(Rb)}{c^2} \right]$$

$$+ \left[a_0^2 \left[\cos \beta_1^0 + \phi_x^0 \right] \frac{d}{dx} \ln \left[1 / \frac{(Rb)^0}{c^2} \right] \right] \cdot \Delta \frac{(Rb)}{c^2} \qquad \text{(A-18)}$$

APPENDIX B
BOUNDARY CONDITIONS FOR PERTURBATION DISTURBANCE POTENTIALS

This appendix contains the perturbation boundary conditions associated with various parameter perturbations of the quasi three-dimensional full potential base flow formulation described in Section 2.4.2. These include variations in maximum blade thickness, blade spacing, inflow Mach number, inflow angle, maximum blade camber, and blade stagger. In addition, special forms of these for maximum blade thickness, blade spacing, and inflow Mach number perturbations based on the transonic small-disturbance formulation for an unstaggered cascade are also presented.

The coordinate system employed for the disturbance full potential formulation is sketched below.

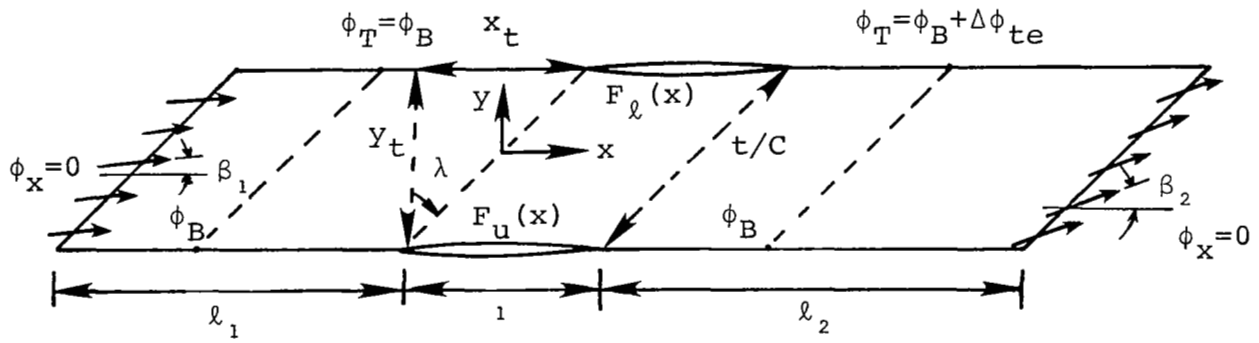

In this figure, $F_u(x)$, $F_\ell(x)$ denote the dimensionless ordinates of the blade upper and lower surface and are given in normalized form by

$$F_u(x) = \tau\bar{f}(x) + h\bar{g}(x) \tag{B-1}$$

$$F_\ell(x) = -\tau\bar{f}(x) + h\bar{g}(x) \tag{B-2}$$

where τ and h represent the thickness ratio and maximum camber, and $(\bar{f}(x), \bar{g}(x))$ are the corresponding normalized thickness and camber distributions. The normalized quantities (x_t, y_t) are related to the blade spacing t and stagger angle λ by

$$x_t = \frac{t}{C}\sin\lambda$$
$$y_t = \frac{t}{C}\cos\lambda \tag{B-3}$$

and (β_1, β_2) are the uniform inflow and outflow angles, respectively, of the absolute flow. It is convenient to define the quantities:

$$x_1 = x + \frac{x_t}{2}$$

$$x_2 = x - \frac{x_t}{2}$$

$$y_1 = \frac{y_t}{2} \qquad \text{(B-4)}$$

$$y_2 = -\frac{y_t}{2}$$

$$x_1^0 = x + \frac{x_t^0}{2}; \text{ etc.}$$

The appropriate boundary conditions for both the base flow ϕ^0 and the perturbation component ϕ^1 for various perturbations are as follows:

1. Blade thickness ratio perturbation

$$\tau = \tau^0 + \Delta\tau \qquad \text{(B-5)}$$

Blade surface condition: $0 \leq x \leq 1$

$$\phi_y^0(x_1, y_1) = \left[-\tau^0 \bar{f}'(x) + h\bar{g}'(x)\right] \cos\beta_1 - \sin\beta_1$$

$$\phi_y^0(x_2, y_2) = \left[\tau^0 \bar{f}'(x) + h\bar{g}'(x)\right] \cos\beta_1 - \sin\beta_1$$

$$\phi_y^1(x_1, y_1) = -\Delta\tau \bar{f}'(x) \cos\beta_1$$

$$\phi_y^1(x_2, y_2) = \Delta\tau \bar{f}'(x) \cos\beta_1 \qquad \text{(B-6)}$$

Periodic condition: $-\ell_1 < x < 0$

$$\phi^0(x_1, y_1) = \phi^0(x_2, y_2)$$

$$\phi^1(x_1, y_1) = \phi^1(x_2, y_2) \qquad \text{(B-7)}$$

Cyclic condition: $1 < x < 1 + \ell_2$

$$\phi^0(x_1, y_1) = \phi^0(x_2, y_2) + \Delta\phi^0_{te}$$

$$\phi^1(x_1, y_1) = \phi^1(x_2, y_2) + \Delta\phi^1_{te} \qquad \text{(B-8)}$$

2. Blade spacing perturbation

$$\frac{t}{C} = \frac{t^0}{C} + \frac{\Delta t}{C} \qquad \text{(B-9)}$$

Blade surface condition: $0 \leq x \leq 1$

$$\phi^0_y(x^0_1, y^0_1) = F'_\ell(x) \cos \beta_1 - \sin \beta_1$$

$$\phi^0_y(x^0_2, y^0_2) = F'_u(x) \cos \beta_1 - \sin \beta_1$$

$$\phi^1_y(x^0_1, y^0_1) = -\left[F''_\ell(x) \cos \beta_1 \sin \lambda^0 + \phi^0_{yy}(x^0_1, y^0_1) \cos \lambda^0\right]\frac{\Delta t}{2C}$$

$$\phi^1_y(x^0_2, y^0_2) = \left[F''_u(x) \cos \beta_1 \sin \lambda^0 + \phi^0_{yy}(x^0_2, y^0_2) \cos \lambda^0\right]\frac{\Delta t}{2C} \qquad \text{(B-10)}$$

Periodic condition: $-\ell_1 < x < 0$

$$\phi^0(x^0_1, y^0_1) = \phi^0(x^0_2, y^0_2)$$

$$\phi^1(x^0_1, y^0_1) = \phi^1(x^0_2, y^0_2) - \left[\phi^0_x(x^0_1, y^0_1) \sin \lambda^0 + \phi^0_y(x^0_1, y^0_1) \cos \lambda^0\right]\frac{\Delta t}{C} \qquad \text{(B-11)}$$

Cyclic condition: $1 < x < 1 + \ell_2$

$$\phi^0(x^0_1, y^0_1) = \phi^0(x^0_2, y^0_2) + \Delta\phi^0_{te}$$

$$\phi^1(x^0_1, y^0_1) = \phi^1(x^0_2, y^0_2) + \Delta\phi^1_{te}$$

Continued on next page

$$+ \left[\phi_x^0(x_2^0(1),\ y_2^0) - \phi_x^0(x_2^0,\ y_2^0)\right] \sin \lambda^0 \frac{\Delta t}{C}$$

$$+ \left[\phi_y^0(x_2^0(1),\ y_2^0) - \phi_y^0(x_2^0,\ y_2^0)\right] \cos \lambda^0 \frac{\Delta t}{C} \qquad \text{(B-12)}$$

where

$$x_1^0(1) = 1 + \frac{x_t^0}{2}, \text{ etc.} \qquad \text{(B-13)}$$

3. Inflow Mach number perturbation

$$M_1 = M_1^0 + \Delta M \qquad \text{(B-14)}$$

Blade surface condition: $0 \le x \le 1$

$$\phi_y^0(x_1,y_1) = F_\ell'(x)\cos \beta_1 - \sin \beta_1$$

$$\phi_y^0(x_2,y_2) = F_u'(x)\cos \beta_1 - \sin \beta_1$$

$$\phi_y^1(x_1,y_1) = 0$$

$$\phi_y^1(x_2,y_2) = 0 \qquad \text{(B-15)}$$

Periodic condition: $-\ell_1 < x < 0$

$$\phi^0(x_1,y_1) = \phi^0(x_2,y_2)$$

$$\phi^1(x_1,y_1) = \phi^1(x_2,y_2) \qquad \text{(B-16)}$$

Cyclic condition: $1 < x < 1 + \ell_2$

$$\phi^0(x_1,y_1) = \phi^0(x_2,y_2) + \Delta\phi_{te}^0$$

$$\phi^1(x_1,y_1) = \phi^1(x_2,y_2) + \Delta\phi_{te}^1 \qquad \text{(B-17)}$$

4. Inflow angle perturbation

$$\beta_1 = \beta_1^0 + \Delta\beta_1 \tag{B-18}$$

Blade surface condition: $0 \le x \le 1$

$$\phi_y^0(x_1,y_1) = F_\ell'(x)\cos\beta_1^0 - \sin\beta_1^0$$

$$\phi_y^0(x_2,y_2) = F_u'(x)\cos\beta_1^0 - \sin\beta_1^0$$

$$\phi_y^1(x_1,y_1) = -\Delta\beta_1 F_\ell'(x)\sin\beta_1^0$$

$$\phi_y^1(x_2,y_2) = \Delta\beta_1 F_u'(x)\sin\beta_1^0 \tag{B-19}$$

Periodic condition: $-\ell_1 < x < 0$

$$\phi^0(x_1,y_1) = \phi^0(x_2,y_2)$$

$$\phi^1(x_1,y_1) = \phi^1(x_2,y_2) \tag{B-20}$$

Cyclic condition: $1 < x < 1 + \ell_2$

$$\phi^0(x_1,y_1) = \phi^0(x_2,y_2) + \Delta\phi_{te}^0$$

$$\phi^1(x_1,y_1) = \phi^1(x_2,y_2) + \Delta\phi_{te}^1 \tag{B-21}$$

5. Blade maximum camber perturbation

$$h = h^0 + \Delta h \tag{B-22}$$

Blade surface condition: $0 \le x \le 1$

$$\phi_y^0(x_1,y_1) = [-\tau\bar{f}'(x) + h^0\bar{g}'(x)]\cos\beta_1 - \sin\beta_1$$

$$\phi_y^0(x_2,y_2) = [\tau\bar{f}'(x) + h^0\bar{g}'(x)]\cos\beta_1 - \sin\beta_1$$

Continued on next page

$$\phi_y^1(x_1,y_1) = \Delta h\bar{g}'(x) \cos \beta_1$$

$$\phi_y^1(x_2,y_2) = \Delta h\bar{g}'(x) \cos \beta_1 \qquad \text{(B-23)}$$

Periodic condition: $-\ell_1 < x < 0$

$$\phi^0(x_1,y_1) = \phi^0(x_2,y_2)$$

$$\phi^1(x_1,y_1) = \phi^1(x_2,y_2) \qquad \text{(B-24)}$$

Cyclic condition: $1 < x < \ell_2$

$$\phi^0(x_1,y_1) = \phi^0(x_2,y_2) + \Delta\phi_{te}^0$$

$$\phi^1(x_1,y_1) = \phi^1(x_2,y_2) + \Delta\phi_{te}^1 \qquad \text{(B-25)}$$

6. Blade stagger angle perturbation

$$\lambda = \lambda^0 + \Delta\lambda \qquad \text{(B-26)}$$

Blade surface condition: $0 \le x \le 1$

$$\phi_y^0(x_1^0,y_1^0) = F_\ell'(x) \cos \beta_1 - \sin \beta_1$$

$$\phi_y^0(x_2^0,y_2^0) = F_u'(x) \cos \beta_1 - \sin \beta_1$$

$$\phi_y^1(x_1^0,y_1^0) = \left[- \phi_{xy}^0(x_1^0,y_1^0) \cos \lambda^0 + \phi_{xy}^0(x_1^0,y_1^0) \sin \lambda^0 \right] \frac{t}{2C} \Delta\lambda$$

$$\phi_y^1(x_2^0,y_2^0) = \left[\phi_{xy}^0(x_2^0,y_2^0) \cos \lambda^0 - \phi_{xy}^0(x_2^0,y_2^0) \sin \lambda^0 \right] \frac{t}{2C} \Delta\lambda \qquad \text{(B-27)}$$

Periodic condition: $-\ell_1 < x < 0$

$$\phi^0(x_1^0,y_1^0) = \phi^0(x_2^0,y_2^0)$$

$$\phi^1(x_1^0,y_1^0) = \phi^1(x_2^0,y_2^0) - \left[\phi_x^0(x_1^0,y_1^0)\cos\lambda^0 - \phi_y^0(x_2^0,y_2^0)\sin\lambda^0\right]\frac{t}{C}\Delta\lambda \qquad \text{(B-28)}$$

Cyclic condition: $1 < x < 1 + \ell_2$

$$\phi^0(x_1^0,y_1^0) = \phi^0(x_2^0,y_2^0) + \Delta\phi_{te}^0$$

$$\phi^1(x_1^0,y_1^0) = \phi^1(x_2^0,y_2^0) + \Delta\phi_{te}^1 + \left[\phi_x^0(x_2^0(1),y_2^0) - \phi_x^0(x_2^0,y_2^0)\right]\frac{t}{C}\cos\lambda^0\Delta\lambda - \left[\phi_y^0(x_2^0(1),y_2^0) - \phi_y^0(x_2^0,y_2^0)\right]\frac{t}{C}\sin\lambda^0\Delta\lambda \qquad \text{(B-29)}$$

For an unstaggered cascade, the special forms of the boundary conditions for the perturbations given above follow directly. However, for an unstaggered nonlifting cascade, the additional symmetry of the flow provides a convenient alternative specification to the Dirichlet-type periodic and cyclic boundary conditions previously derived. This is, of course, based on the fact that the horizontal boundaries extending fore and aft of the blades, due to the flow symmetry, become dividing streamlines so that a Neumann condition of no normal flow can be specified. The basic form of the boundary conditions for the disturbance potential ϕ then become

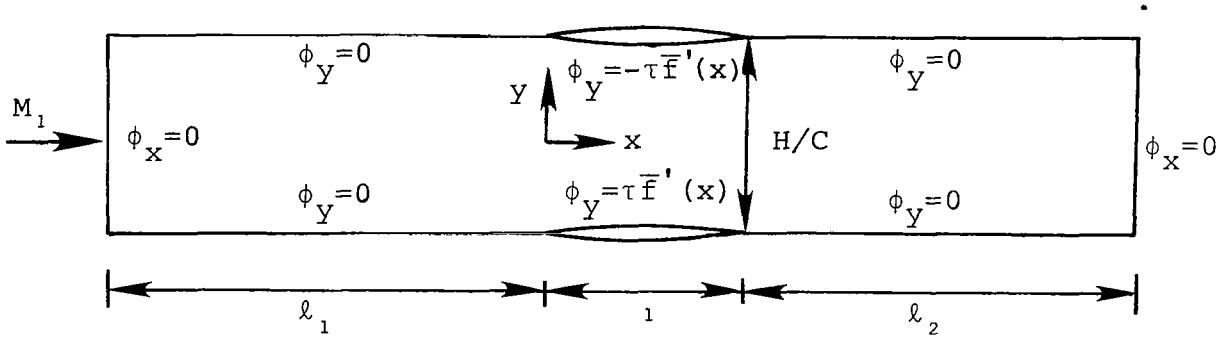

This leads to the following boundary conditions for the perturbation problems associated with thickness ratio τ, spacing ratio H/C, and free stream Mach number M_1 changes.

1. Thickness ratio perturbation

$$\tau = \tau^0 + \Delta\tau \tag{B-30}$$

Blade surface condition: $0 \le x \le 1$

$$\phi_y^1\left(x, \frac{H}{2C}\right) = -\Delta\tau\bar{f}'(x)$$

$$\phi_y^1\left(x, -\frac{H}{2C}\right) = \Delta\tau\bar{f}'(x) \tag{B-31}$$

Dividing streamlines: $-\ell_1 < x < 0, \quad 1 < x < 1 + \ell_2$

$$\phi_y^1\left(x, \frac{H}{2C}\right) = \phi_y^1\left(x, -\frac{H}{2C}\right) = 0 \tag{B-32}$$

2. Spacing ratio perturbation

$$\frac{H}{C} = \frac{H^0}{C} + \frac{\Delta H}{C} \tag{B-33}$$

Blade surface condition: $0 \le x \le 1$

$$\phi_y^1\left(x, \frac{H^0}{2C}\right) = -\phi_{yy}^0\left(x, \frac{H^0}{2C}\right)\frac{\Delta H}{2C}$$

$$\phi_y^1\left(x, -\frac{H^0}{2C}\right) = \phi_{yy}^0\left(x, -\frac{H^0}{2C}\right)\frac{\Delta H}{2C} \tag{B-34}$$

Dividing streamlines: $-\ell_1 < x < 0, \quad 1 < x < 1 + \ell_2$

$$\phi_y^1\left(x, \frac{H^0}{2C}\right) = -\phi_{yy}^0\left(x, \frac{H^0}{2C}\right)\frac{\Delta H}{2C}$$

$$\phi_y^1\left(x, -\frac{H^0}{2C}\right) = \phi_{yy}^0\left(x, -\frac{H^0}{2C}\right)\frac{\Delta H}{2C} \tag{B-35}$$

3. Inflow Mach number perturbation

$$M_1 = M_1^0 + \Delta M_1 \tag{B-36}$$

Blade surface condition: $0 \le x \le 1$

$$\phi_y^1\left(x, \frac{H}{2C}\right) = 0$$

$$\phi_y^1\left(x, -\frac{H}{2C}\right) = 0 \tag{B-37}$$

Dividing streamlines: $-\ell_1 < x < 0, \quad 1 < x < 1 + \ell_2$

$$\phi_y^1\left(x, \frac{H}{2C}\right) = 0$$

$$\phi_y^1\left(x, -\frac{H}{2C}\right) = 0 \tag{B-38}$$

For the Mach number perturbation, the perturbation boundary conditions are homogeneous but the differential equation is not. For the transonic small-disturbance approximation, instead of the perturbation equation given by equation (36), we have instead the following equation.

$$\left\{\left[1 - M_1^2 - M_1^2(\gamma+1)\phi_x^0\right]\phi_x^1\right\}_x + \left(\phi_y^1\right)_y = 2M_1\phi_{xx}^0\Delta M_1 \tag{B-39}$$

APPENDIX C

LIST OF SYMBOLS

a	local speed of sound, m/sec; eq. (7)
$\bar{A}$	coefficient of ϕ^1_{xx} in perturbation disturbance potential differential equation (11); defined by eq. (A-13)
b	stream sheet thickness, m
$\bar{B}$	coefficient of ϕ^1_{xy} in perturbation disturbance potential differential equation (11); defined by eq. (A-14)
C	blade chord, m
$\bar{C}$	coefficient of ϕ^1_{yy} in perturbation disturbance potential differential equation (11); defined by eq. (A-15)
C_p	pressure coefficient, $(p-p_1)/\frac{1}{2}\rho_1 U_1^2$
$\bar{D}$	coefficient of ϕ^1_x in perturbation disturbance potential differential equation (11); defined by eq. (A-16)
E	total energy per unit mass, m^2/sec^2; eq. (2)
E_r	relative total energy per unit mass, m^2/sec^2; eq. (2)
$\bar{E}$	coefficient of ϕ^1_y in perturbation disturbance potential differential equation (11); defined by eq. (A-17)
$\bar{f}$	nondimensional ordinates of blade thickness; normalized by τC
F_u, F_ℓ	nondimensional ordinates of the blade upper and lower surfaces, respectively; normalized by C
$\bar{F}$	right-hand-side of perturbation disturbance potential differential equation (11); defined by eq. (A-18)
$\bar{g}$	normalized ordinates of blade mean camber line; normalized by hC
h	blade maximum camber ratio; i.e., maximum height of mean camber line normal to chord divided by chord

H	total enthalpy per unit mass, m^2/sec^2; eq. (2): also, blade spacing for nonstaggered cascades, m
H_r	relative total enthalpy (rothalpy) per unit mass, m^2/sec^2; eq. (2)
K	transonic small-disturbance similarity parameter; eq. (34)
ℓ_1	nondimensional length denoting distance from blade leading edge to upstream boundary, normalized by C
ℓ_2	nondimensional length denoting distance from blade trailing edge to downstream boundary, normalized by C
m	curvilinear blade-fixed coordinate denoting downstream direction, m
M_1	absolute inlet Mach number
p	static pressure, Newton/m^2
q_1	uniform inlet velocity, m/sec
q_2	uniform outlet velocity, m/sec
Q	approximate perturbed flow solution for arbitrary flow quantity, eq. (3)
Q_o	base flow solution for arbitrary flow quantity, eq. (3)
Q_p	linearized perturbation solution per unit perturbation change for arbitrary flow quantity, eq. (3)
R	stream sheet radius of blade-to-blade surface, m
t	blade spacing in θ direction, m
U	relative velocity component in blade-fixed m-coordinate direction, m/sec
V	relative velocity component in blade-fixed θ-coordinate direction, m/sec
v_n	relative velocity-component normal to blade surface in blade-fixed coordinate system, m/sec
(x,y)	nondimensional blade-fixed coordinates related to the (m,θ) coordinate system by eq. (8), normalized by C

(x_t, y_t) nondimensional blade spacing quantities defined by eq. (12)

$\tilde{y}$ nondimensional transonically scaled y-coordinate, defined by eq. (31)

β_1 absolute inflow angle, radians

β_2 absolute outflow angle, radians

γ ratio of specific heats, equal to 1.4 for air

Δ amplitude of perturbation of geometric or flow parameter

Θ absolute angular coordinate, defined in figure 2; radians

λ blade setting or stagger angle, radians

ρ density, kg/m^3

τ blade thickness ratio; i.e., maximum blade thickness normal to chord divided by chord

ϕ dimensionless disturbance velocity potential, normalized by Cq_1; eq. (8)

ϕ^0 dimensionless base flow disturbance velocity potential, normalized by Cq_1; eq. (10)

ϕ_1^1 dimensionless perturbation disturbance velocity potential, normalized by Cq_1; eq. (10)

$\tilde{\phi}$ dimensionless transonic small-disturbance velocity potential, normalized by Cq_1; eq. (32)

$\tilde{\phi}^0$ dimensionless base flow transonic small-disturbance velocity potential, normalized by Cq_1; eq. (35)

$\tilde{\phi}^1$ dimensionless perturbation transonic small-disturbance velocity potential, normalized by Cq_1; eq. (35)

$\Delta\phi_{te}$ jump in the disturbance velocity potential at the blade trailing edge

Φ dimensional velocity potential for the complete flow defined in the absolute (nonrotating) reference system; eq. (5), m/sec

Ω rotational speed, radians/sec

Subscripts

u	refers to blade upper surface
ℓ	refers to blade lower surface
1	denotes uniform inlet conditions; also denotes upper boundary of solution domain
2	denotes uniform outlet conditions; also denotes lower boundary of solution domain

Superscripts

0	denotes base flow quantities
1	denotes perturbation quantities

REFERENCES

1. Gopalakrishnan, S. and Bozzola, R.: Computation of Shocked Flows in Compressor Cascades. ASME Paper No. 72-GT-31, Mar. 1972.

2. Kurzrock, J. W. and Novick, A. S.: Transonic Flow Around Rotor Blade Elements. ASME Paper No. 75-FE-24, May 1975.

3. Erdos, J. I., Alzner, E., and McNally, W.: Numerical Solution of Periodic Transonic Flows Through a Fan Stage. AIAA Paper No. 76-369, July 1976.

4. Rae, W. I.: Relaxation Solutions for Three-Dimensional Transonic Flow Through a Compressor Blade Row in the Non-linear Small-Disturbance Approximation. Calspan Rept. No. AB-5487-A-2, Aug. 1976.

5. Hafez, M. M. and Cheng, H. K.: Convergence Acceleration of Relaxation Solutions for Transonic Flow Computations. AIAA Jour., vol. 15, no. 3, Mar. 1977, pp. 329-336.

6. South, J. C., Jr. and Jameson, A.: Relaxation Solutions for Inviscid Axisymmetric Transonic Flow Over Blunt or Pointed Bodies. Proceedings of the AIAA Computational Fluid Dynamics Conference, Palm Springs, CA, 1973, pp. 8-17.

7. Brandt, A.: Multi-level Adaptive Technique (MLAT) for Fast Numerical Solution to Boundary Value Problems. Proceedings of Third International Conference on Numerical Methods in Fluid Mechanics, Paris, 1972, Springer Verlag, NY, 1973, vol. 1, pp. 82-89.

8. Steger, J. L. and Kutler, P.: Implicit Finite-Difference Procedures for the Computation of Vortex Wakes. AIAA Paper No. 76-385, 1976.

9. Beam, R. M. and Warming, R. F.: An Implicit Finite-Difference Algorithm for Hyperbolic Systems in Conservation Law Form. Jour. of Comp. Physics, vol. 22, no. 1, Sept. 1976, pp. 87-110.

10. Chaussee, D. S., Stahara, S. S., and Spreiter, J. R.: Application of an Axisymmetric Implicit Blunt Body Procedure: Computation of Solar Wind Flows Past Terrestrial Planets. AIAA Paper No. 77-700, June 1977.

11. Wu, C. H.: A General Theory of Three-Dimensional Flow in Subsonic and Supersonic Turbomachines of Axial-, Radial, and Mixed-Flow Types, NACA TN 2604, 1952.

12. Erdos, J. and Alzner, E.: Computation of Unsteady Transonic Flows Through Rotating and Stationary Cascades, vol. 1, Method of Analysis. NASA CR-2900, 1977.

13. Alzner, E. and Kalban, P.: Computation of Unsteady Transonic Flows Through Rotating and Stationary Cascades, vol. 2, User's Guide to FORTRAN Program B2DATL. NASA CR-2901, 1977.

14. van Dyke, M.: Perturbation Methods in Fluid Mechanics. The Parabolic Press, Stanford, CA, 1975.

15. Japiske, D.: Review-Progress in Numerical Turbomachinery Analysis. ASME Jour. of Fluids Eng., Dec. 1976, pp. 592-606.

16. Bailey, F. R.: On the Computation of Two- and Three-Dimensional Steady Transonic Flows by Relaxation Methods. VKI Lecture Series "Progress in Numerical Fluid Dynamics," von Kármán Institute for Fluid Dynamics, Rhode-St. Genese, Belgium, Feb. 11-15, 1974.

17. Jameson, A.: Transonic Flow Calculations. VKI Lecture Series 87, "Computational Fluid Dynamics," Mar. 15-19, 1976.

18. Stahara, S. S.: Operational Manual for Two-Dimensional Transonic Code TSFOIL. NEAR TR 94, 1977.

19. Collins, D. J. and Krupp, J. A.: Experimental and Theoretical Investigations in Two-Dimensional Transonic Flow. AIAA Jour., vol. 12, no. 6, pp. 771-778, 1974.

20. Nixon, D.: Perturbation of a Discontinuous Transonic Flow. AIAA Paper No. 77-206, Jan. 1977.

21. Murman, E. M.: Analysis of Embedded Shock Waves Calculated by Relaxation Methods. AIAA Jour., vol. 12, no. 5, pp. 626-633, 1974.

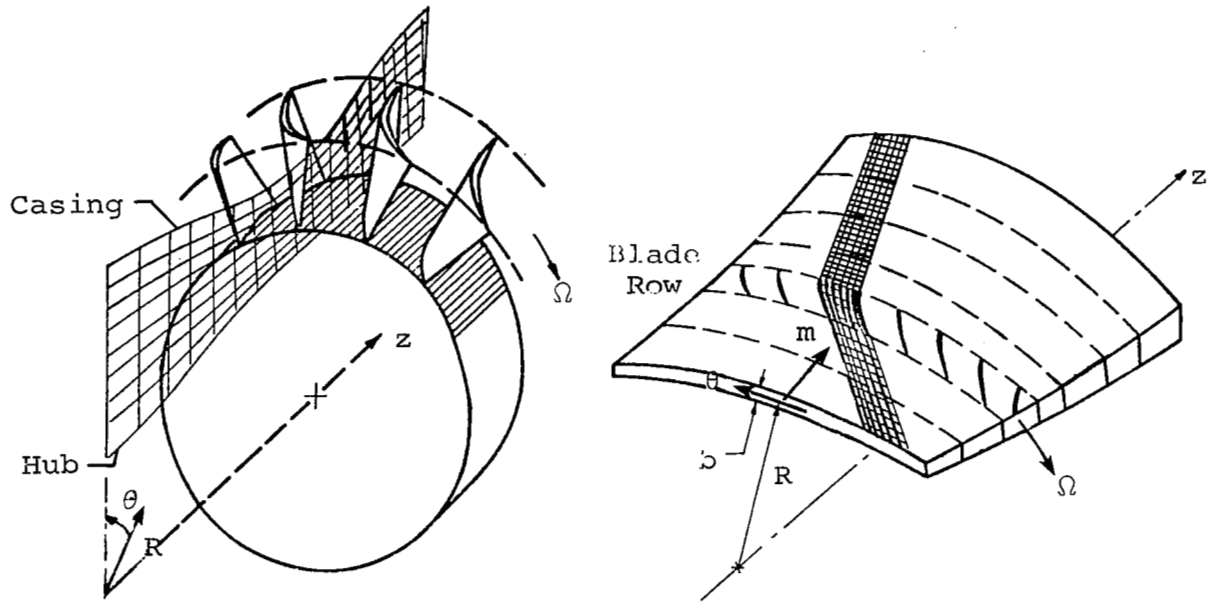

Figure 1.- Coordinate systems for interacting two-dimensional flows used to simulate three-dimensional flow through a single blade row of a turbomachine.

$$x = m$$

$$y = R(\theta - \Omega t)$$

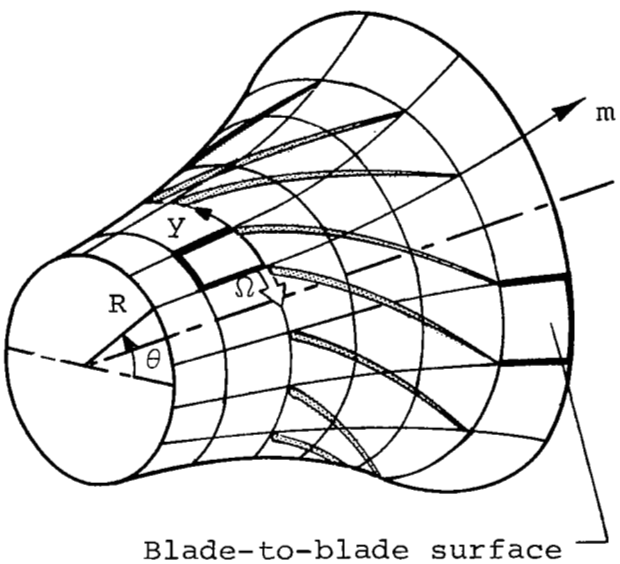

Blade-to-blade surface of revolution

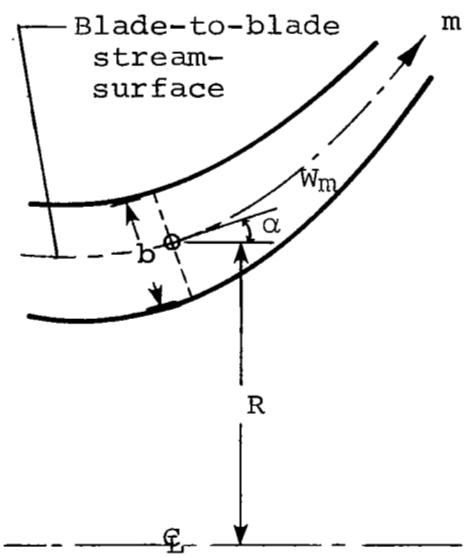

Stream channel in meridional flow plane

Figure 2.- Sketch of blade-to-blade stream surface of revolution with variable stream-sheet thickness b and radius R.

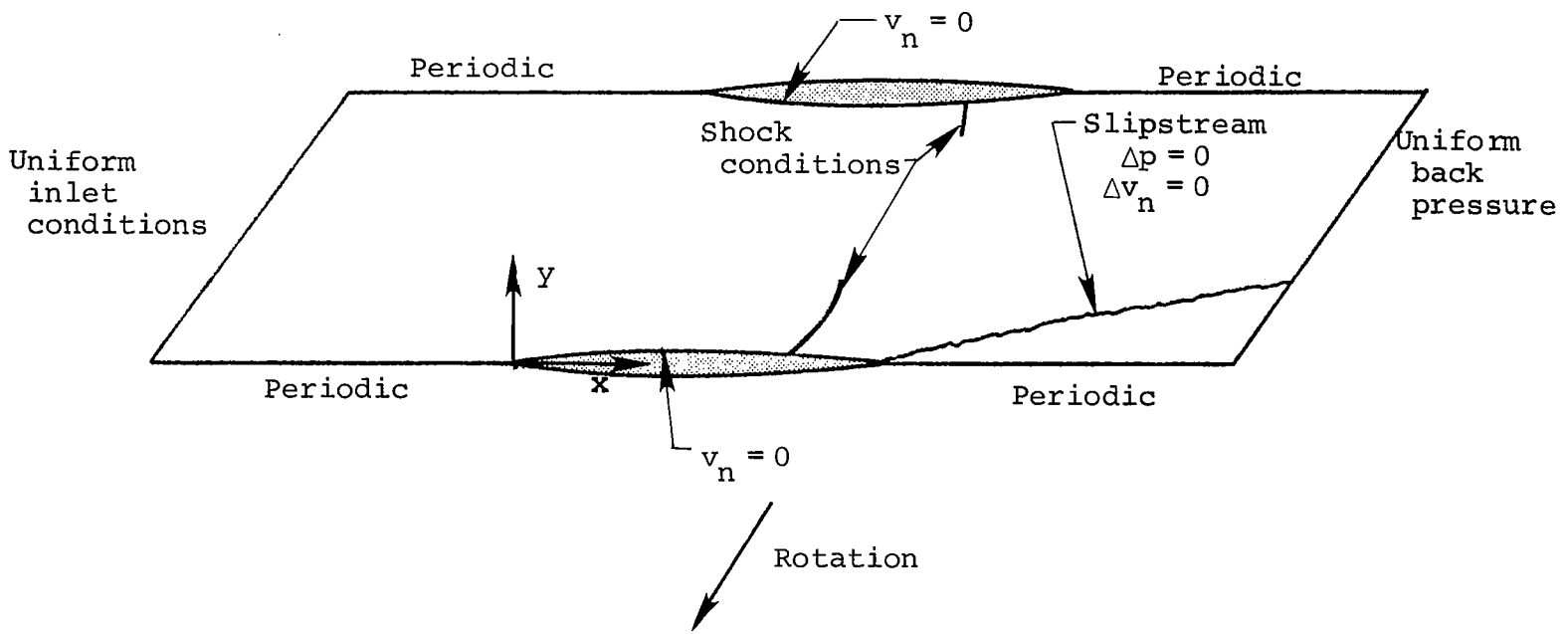

Figure 3.- Boundary conditions for the quasi three-dimensional Euler equation formulation on the curvilinear blade-to-blade stream surface for a system rotating with the blades.

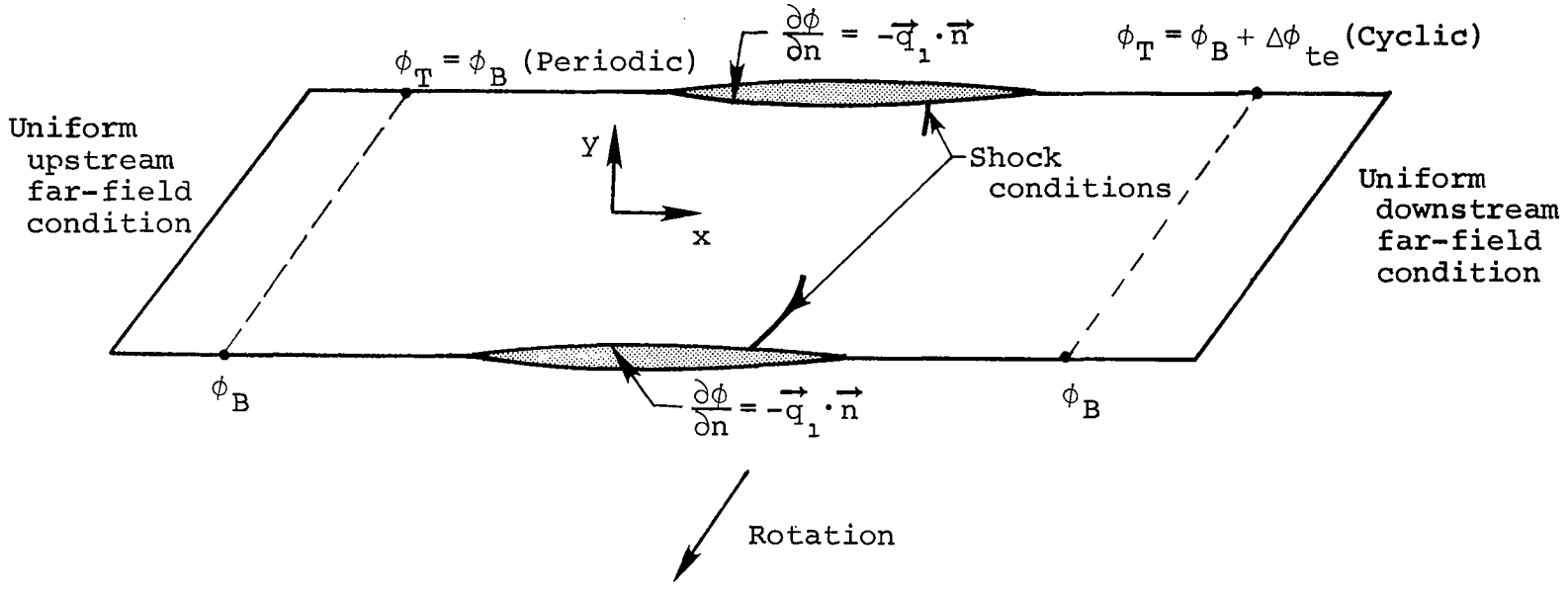

Figure 4.- Boundary conditions for the quasi three-dimensional disturbance full potential formulation on the curvilinear blade-to-blade stream surface for a coordinate system rotating with the blades.

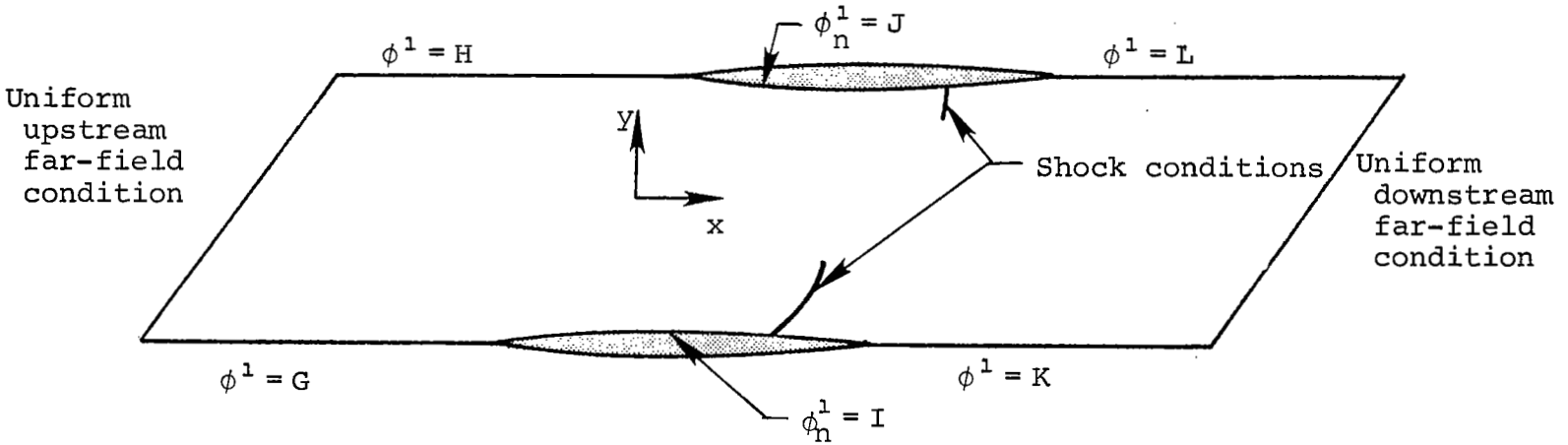

where [G,H,I,J,K,L] are in general functions of $[\phi^o_x, \phi^o_y, \phi^o_{xy}, \phi^o_{yy}, \phi^o_{xx}]$

Figure 5.- General form of the boundary conditions for the perturbation disturbance potential, ϕ^1.

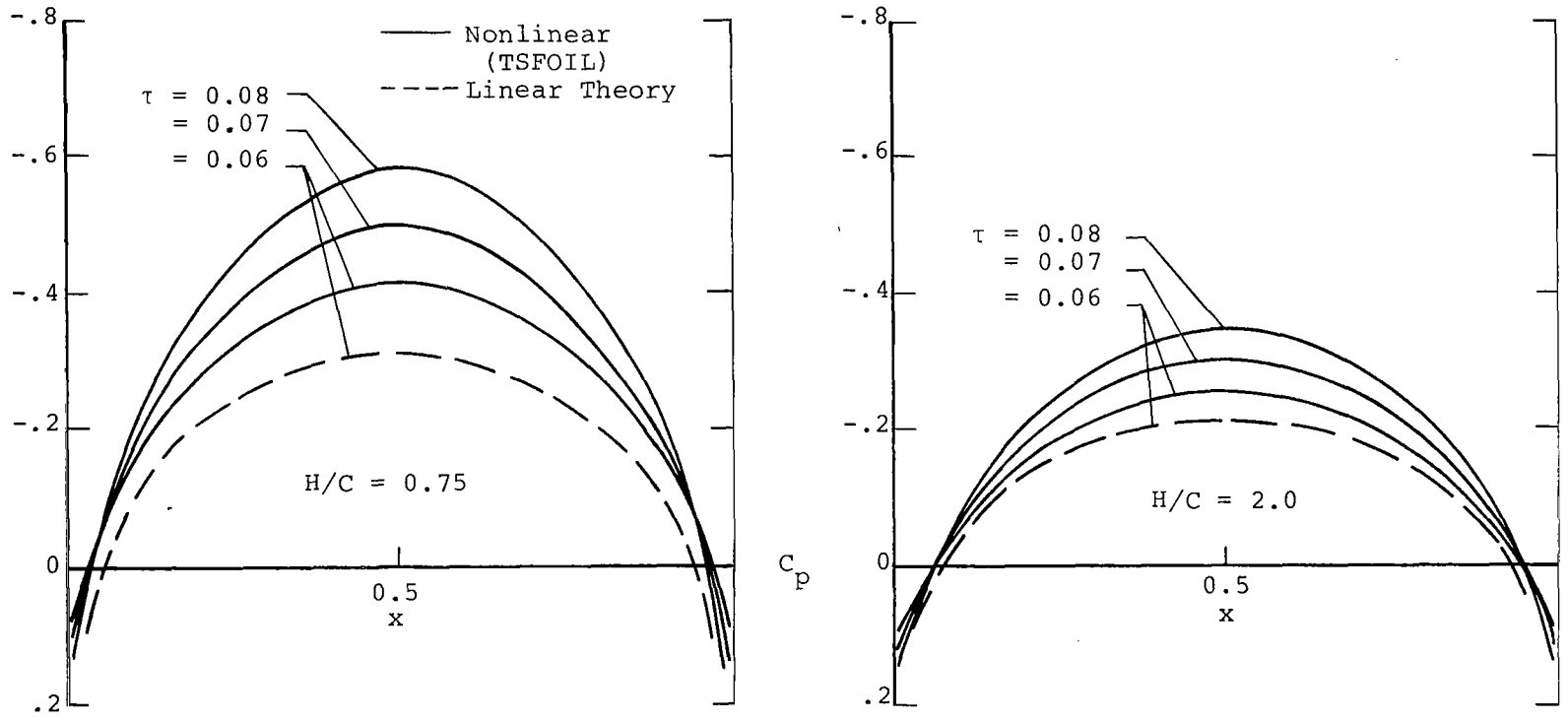

Figure 6.- Surface pressure distributions predicted by TSFOIL for purely subsonic flow past two unstaggered nonlifting cascades of biconvex blade profiles having various thickness ratio with $M_1 = 0.60$.

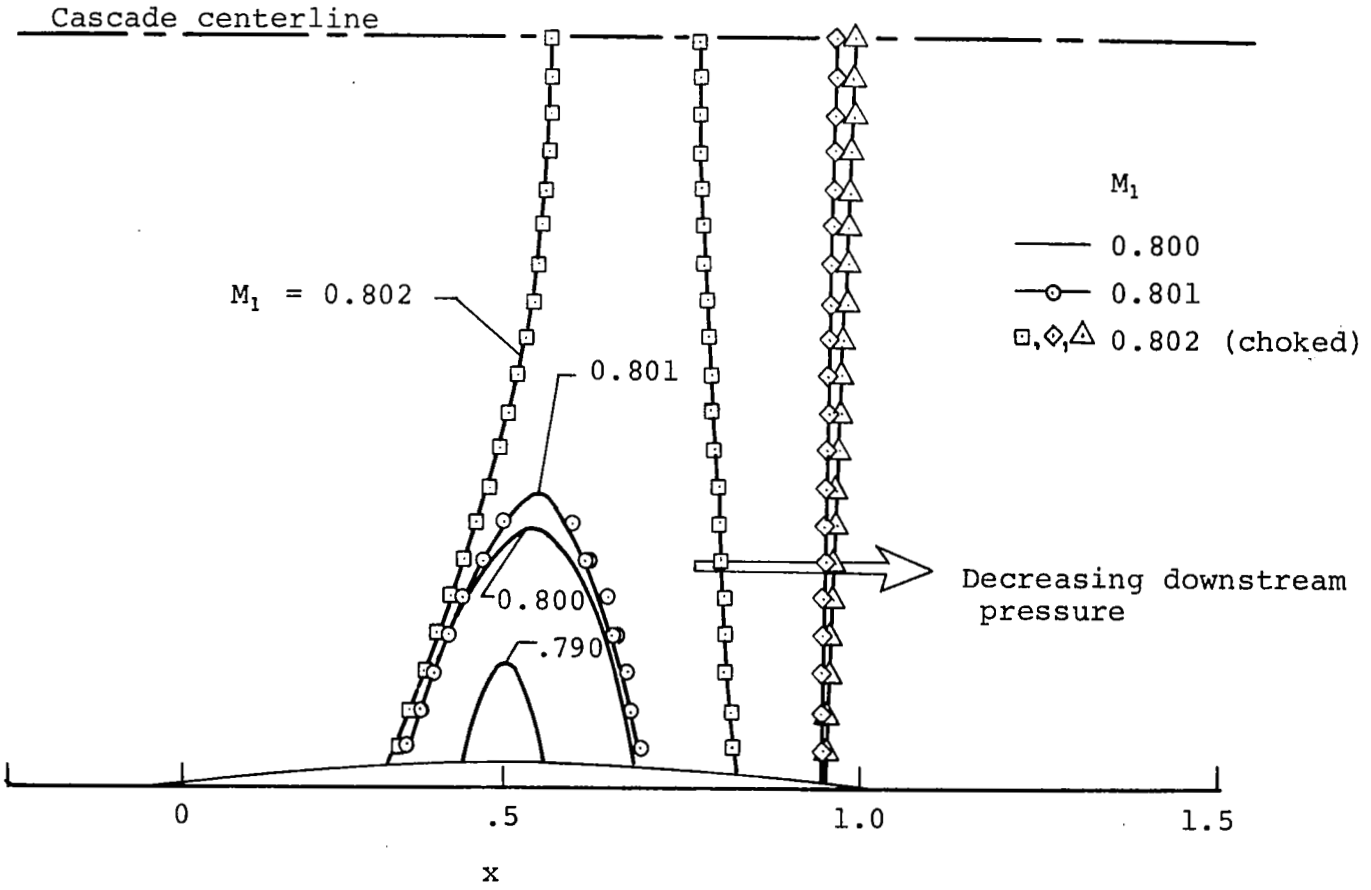

(a) Note small Mach number range between onset of transonic flow and choking.

(b) Choked conditions represent a singular point for the perturbation procedure - can only perturb conditions downstream of the limiting characteristic.

Figure 7.- Location of sonic lines and shock waves during onset of choked flow as predicted by TSFOIL for an unstaggered, nonlifting cascade of parabolic-arc blade profiles with $\tau = 0.07$ and H/C = 2.0.

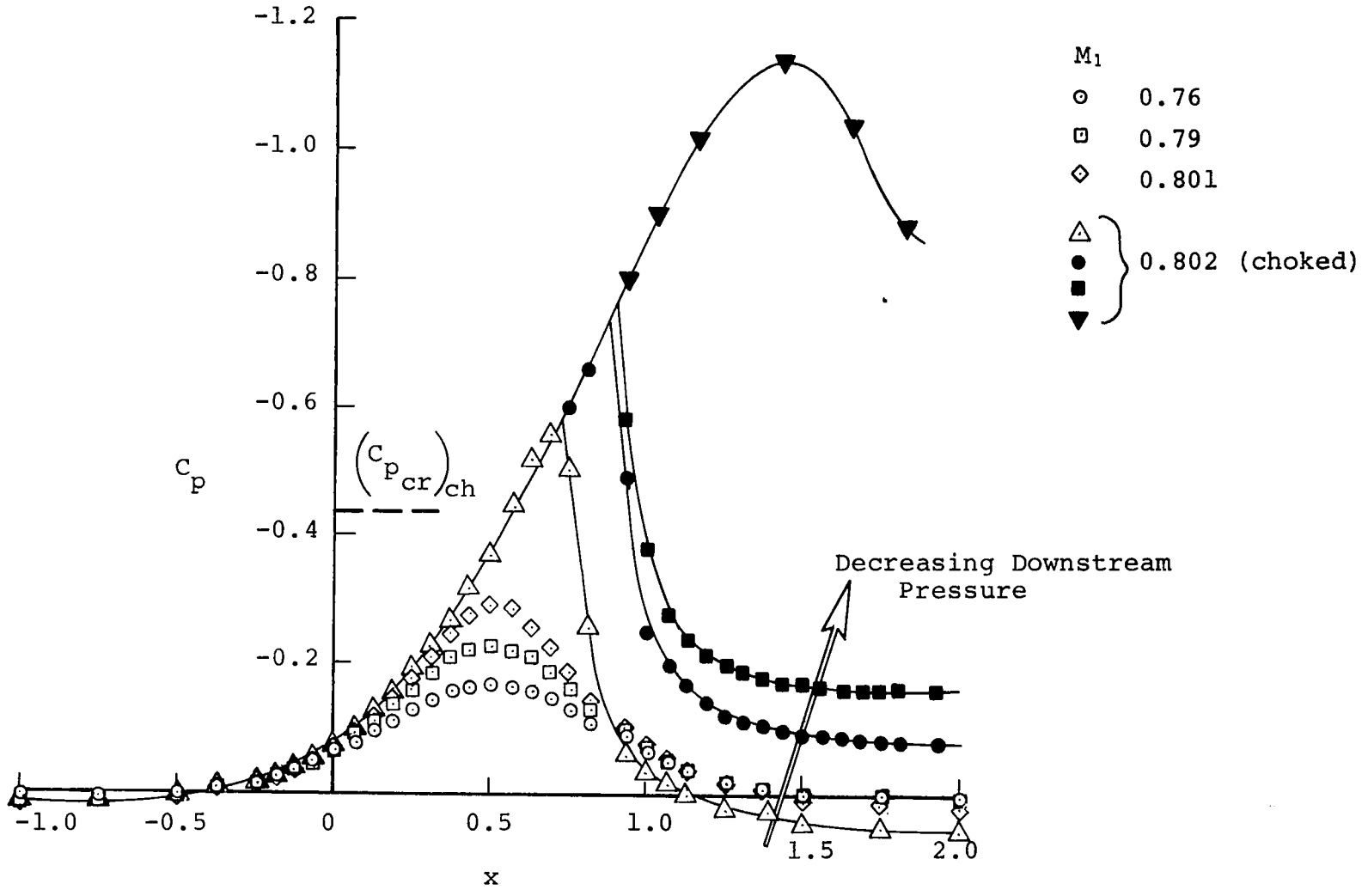

Figure 8.- Pressure distribution on the centerline of the cascade in figure 7 by TSFOIL.

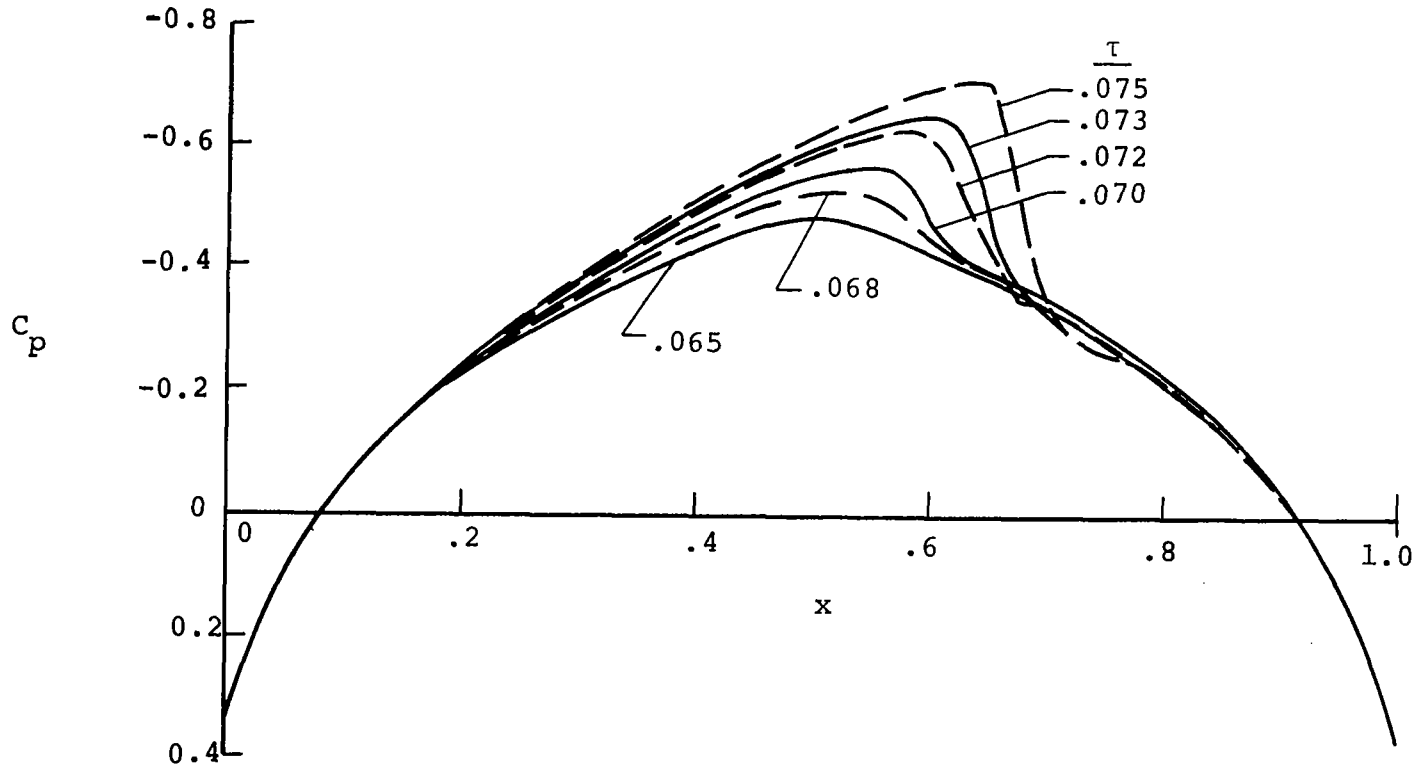

Figure 9.- Surface pressure distributions on an unstaggered nonlifting cascade of parabolic-arc blade profiles for various thickness ratios with $M_1 = 0.80$ and H/C = 2.0 by TSFOIL.

Parabolic- Arc Blades , Unstaggered Nonlifting Cascade, $M_1 = 0.60$
Base Thickness Ratio $\tau = 0.07$, Perturbation Thickness $\Delta\tau = \pm 0.01$

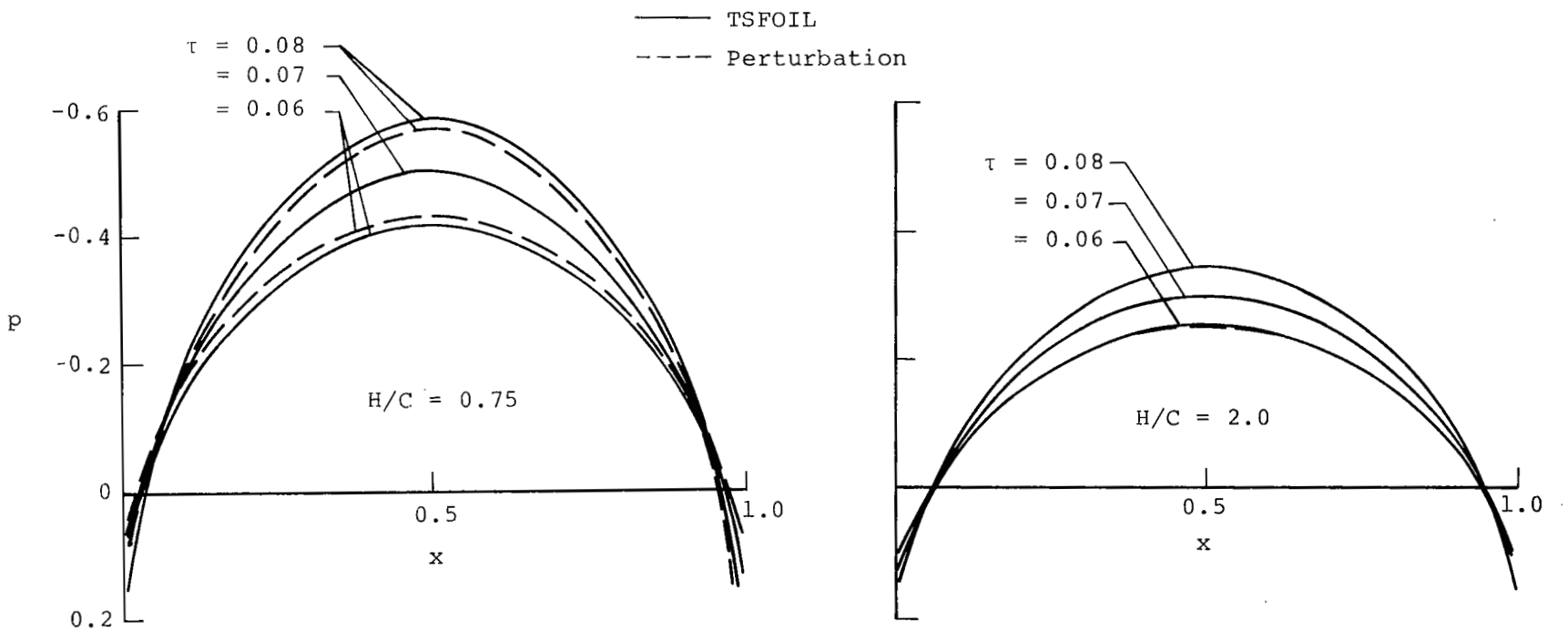

Figure 10.- Subsonic τ perturbation solutions obtained using TSFOIL base solutions and CASCDE perturbation code.

Parabolic-Arc Blades $\tau = 0.07$, Unstaggered Nonlifting Cascade, $M_1 = 0.60$
Base H/C = 0.75, Perturbation $\Delta H/C = \pm 0.10$

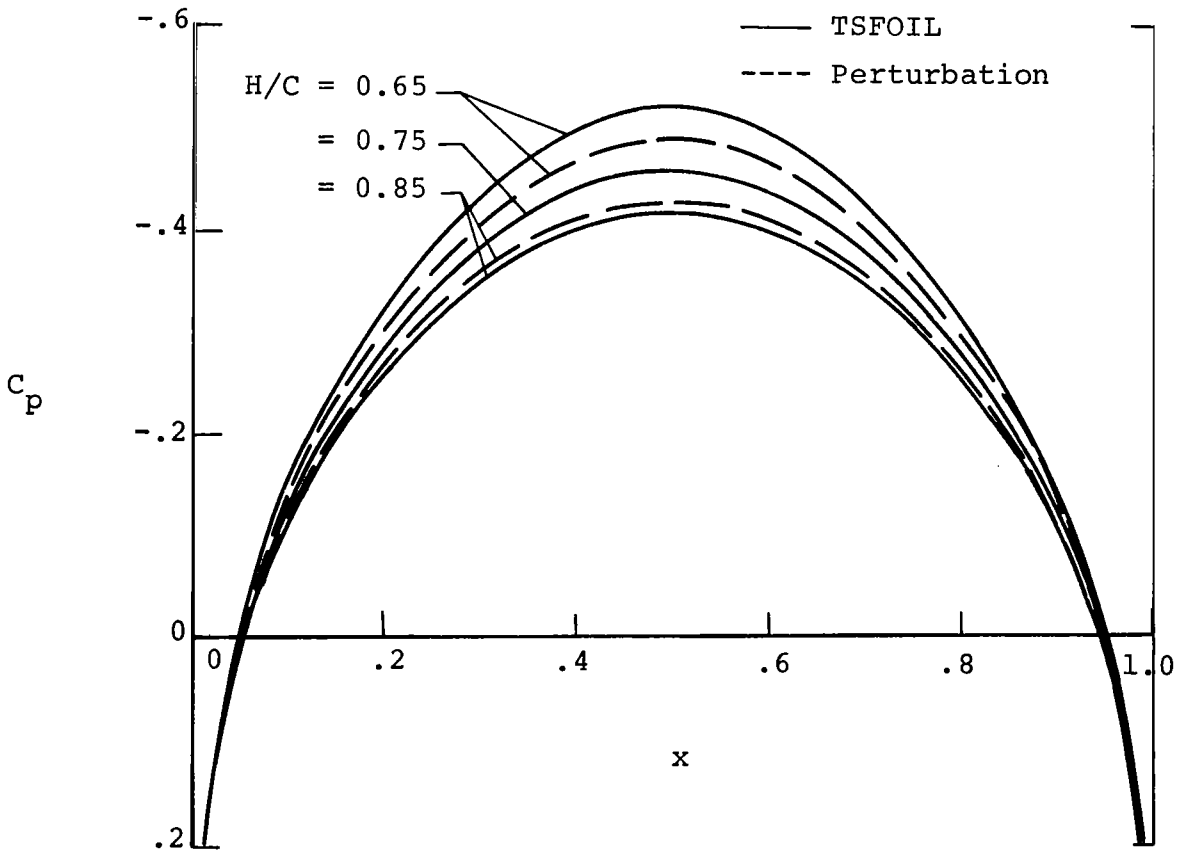

Figure 11.- Subsonic H/C perturbation solutions obtained using TSFOIL base solution and CASCDE perturbation code.

Parabolic- Arc Blades , τ = 0.07, Unstaggered Nonlifting Cascade H/C = 0.75
Base M_1 = 0.60, Perturbation ΔM_1 = -0.10, + 0.05

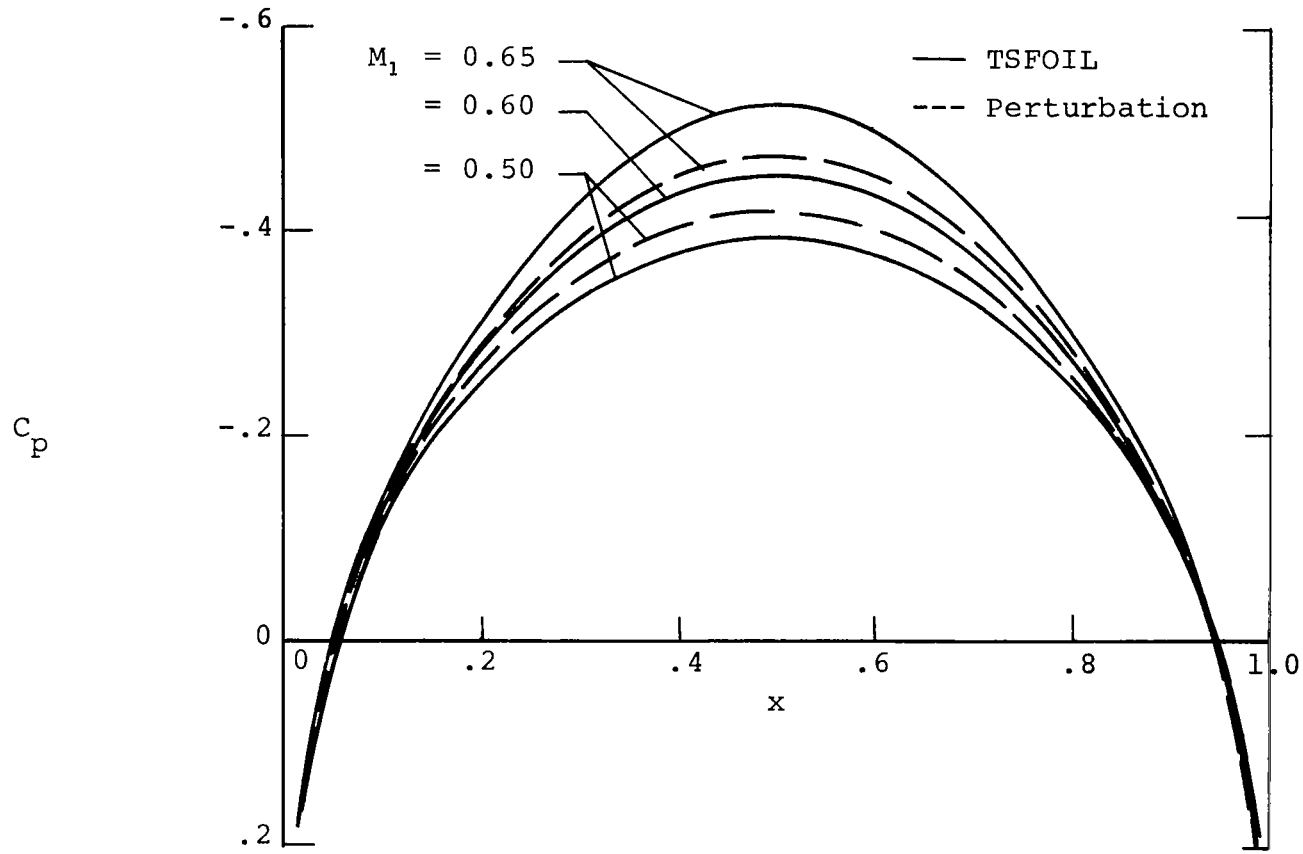

Figure 12.- Subsonic M_1 perturbation solutions obtained using TSFOIL base solution and CASCDE perturbation code.

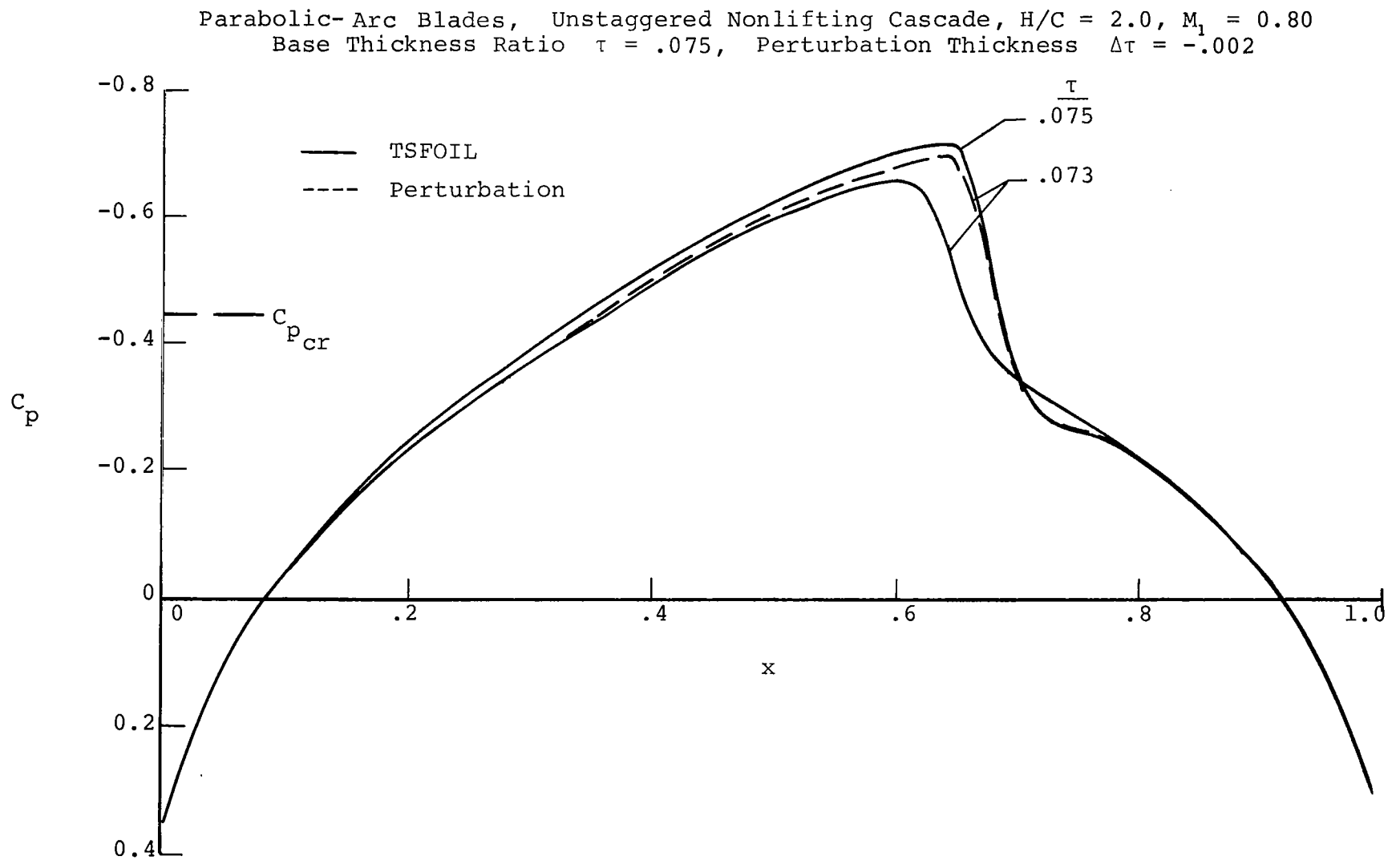

Figure 13.- Supercritical τ perturbation solution obtained using TSFOIL base solution and CASCDE perturbation code.

Parabolic- Arc Blades τ = .075, Unstaggered Nonlifting Cascade, M_1 = .80
Base H/C = 2.0, Perturbation ΔH/C = 0.2

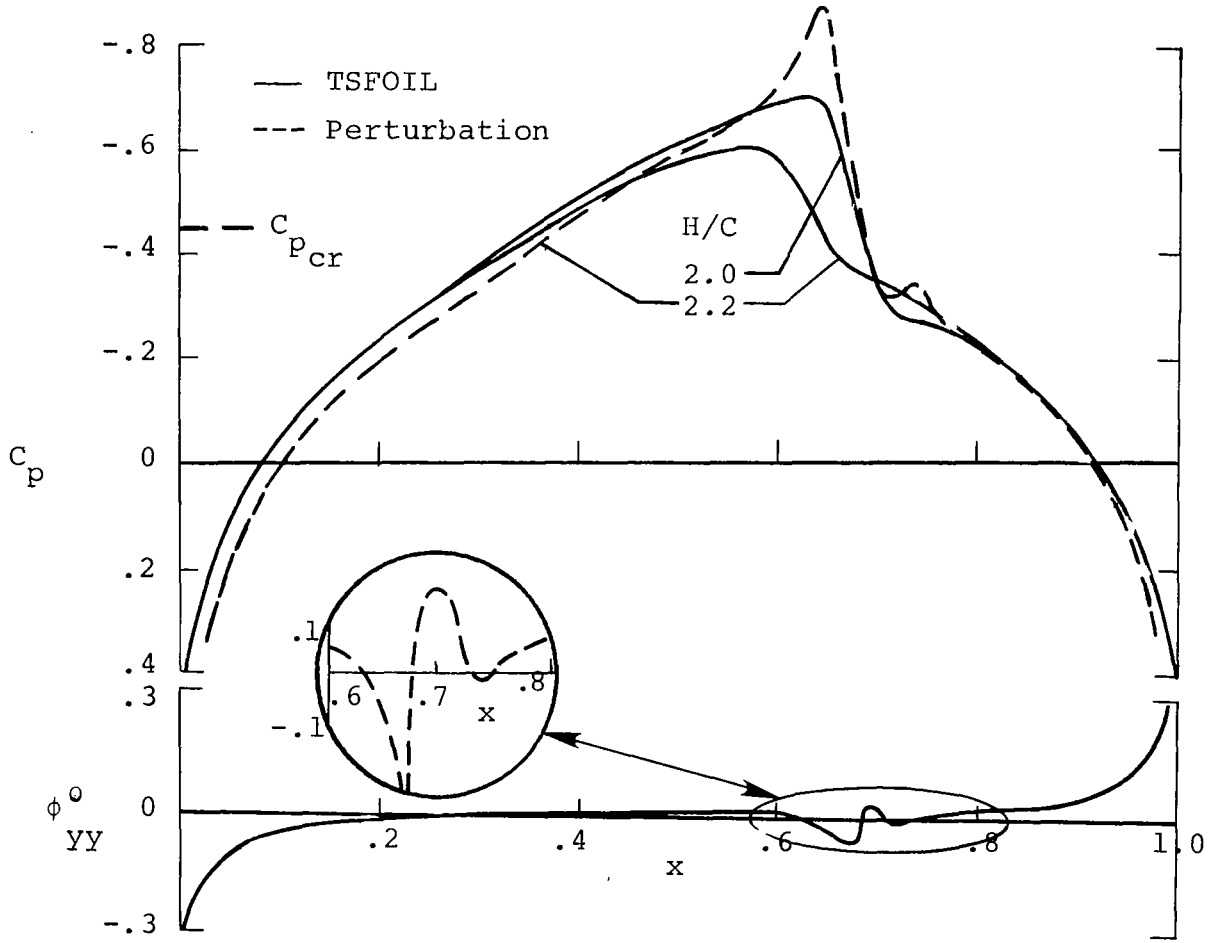

Figure 14.- Supercritical H/C perturbation solution obtained using TSFOIL base solution and CASCDE perturbation code.

Parabolic-Arc Airfoils, Unstaggered Nonlifting Cascade, H/C = 2.0, M_1 = 1.15
Base Thickness Ratio τ = 0.07, Perturbation Thickness $\Delta\tau$ = .005

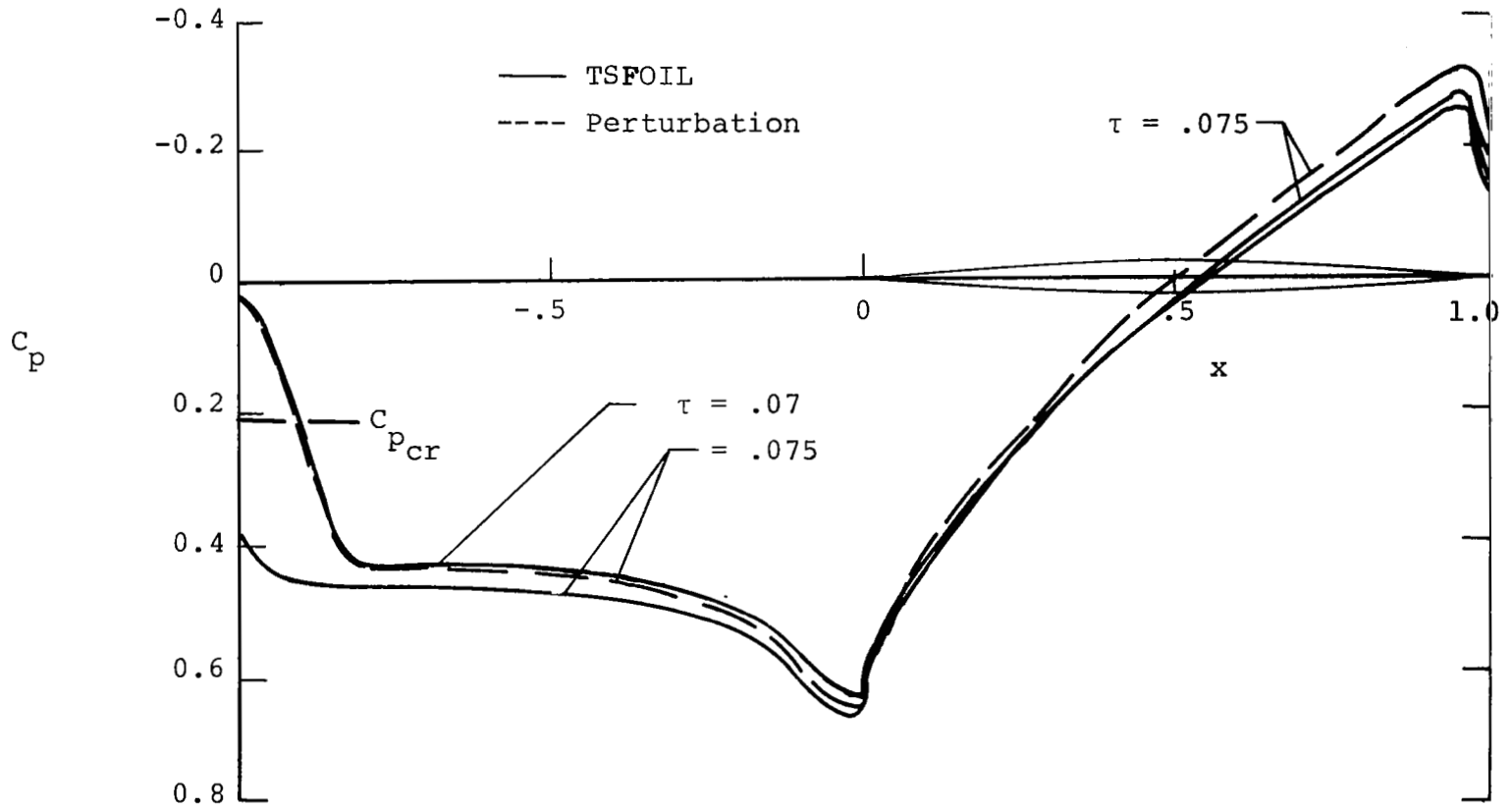

Figure 15.- Supersonic τ perturbation solution obtained using TSFOIL base solution and CASCDE perturbation code.

Parabolic- Arc Blades, τ = 0.07, Unstaggered Nonlifting Cascade, H/C = 2.0
Base M_1 = 1.15, Perturbation ΔM_1 = 0.05

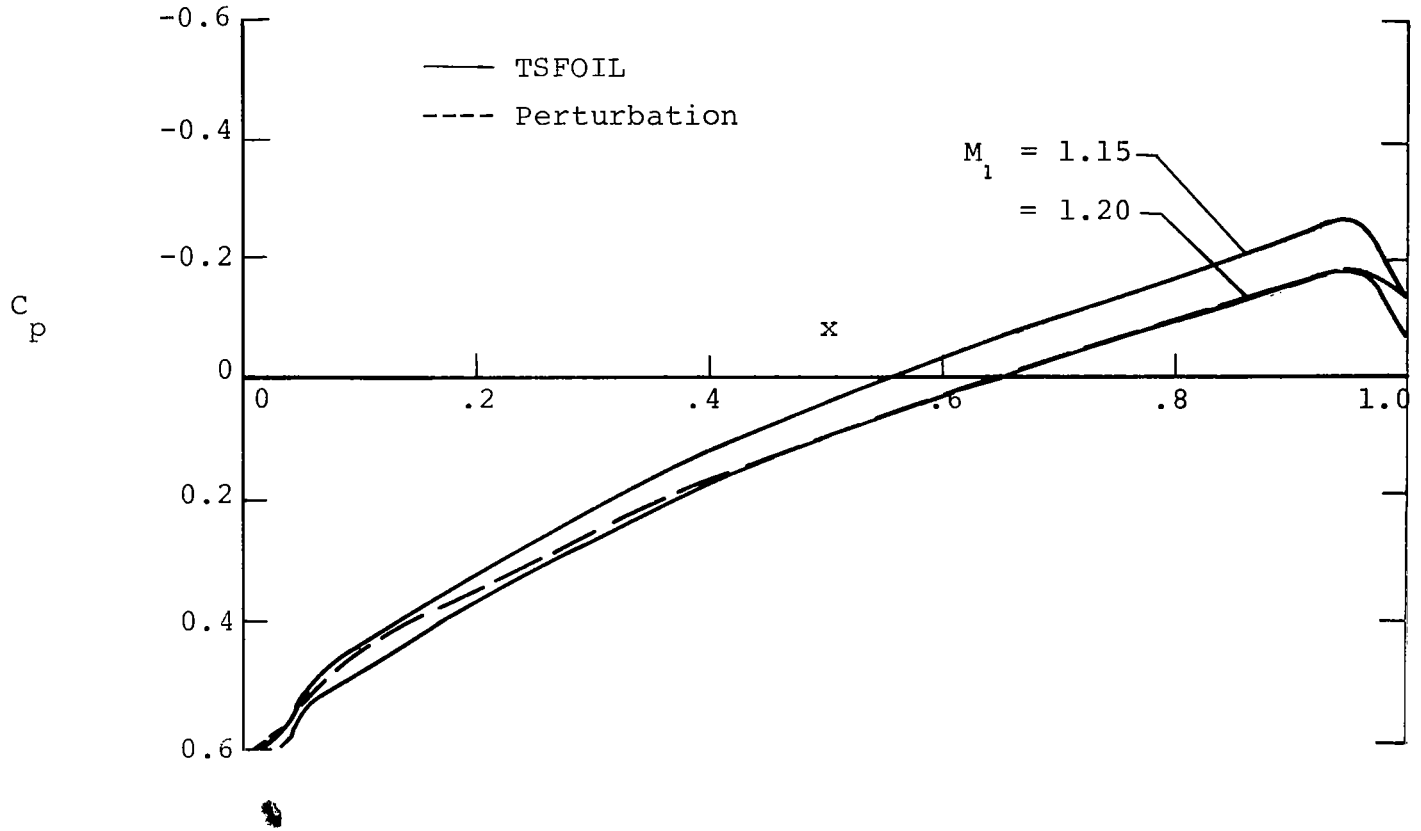

Figure 16.- Supersonic M_1 perturbation solution obtained using TSFOIL base solution and CASCDE perturbation code.

Parabolic-Arc Blades, τ = 0.07, Unstaggered Nonlifting Cascade, H/C = 2.0, M_1 = 0.6

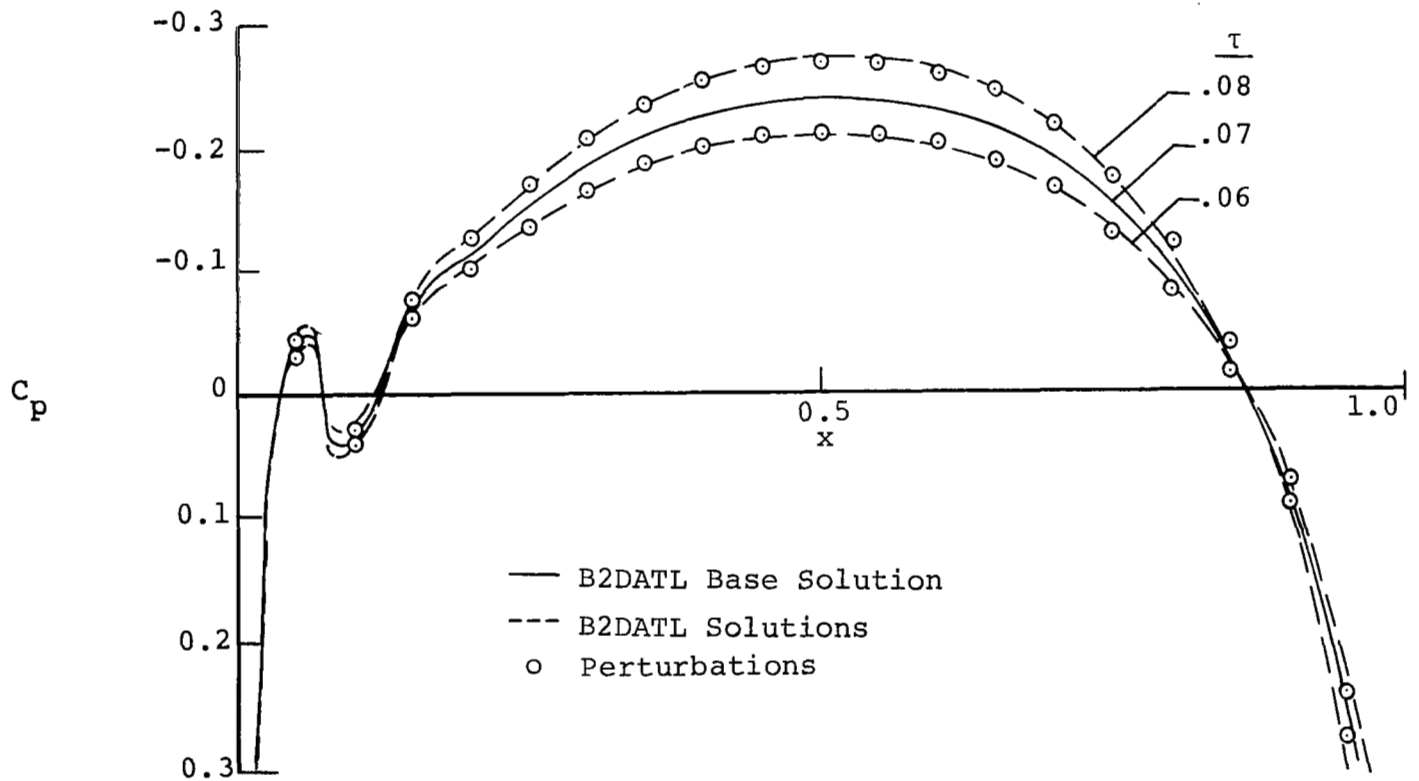

Figure 17.- Subsonic τ perturbation solutions obtained using B2DATL base solution and CASCDE perturbation code.

Parabolic- Arc Blades, Unstaggered Lifting Cascade, H/C = 2.0, β_1 = 4°, M_1 = 0.6

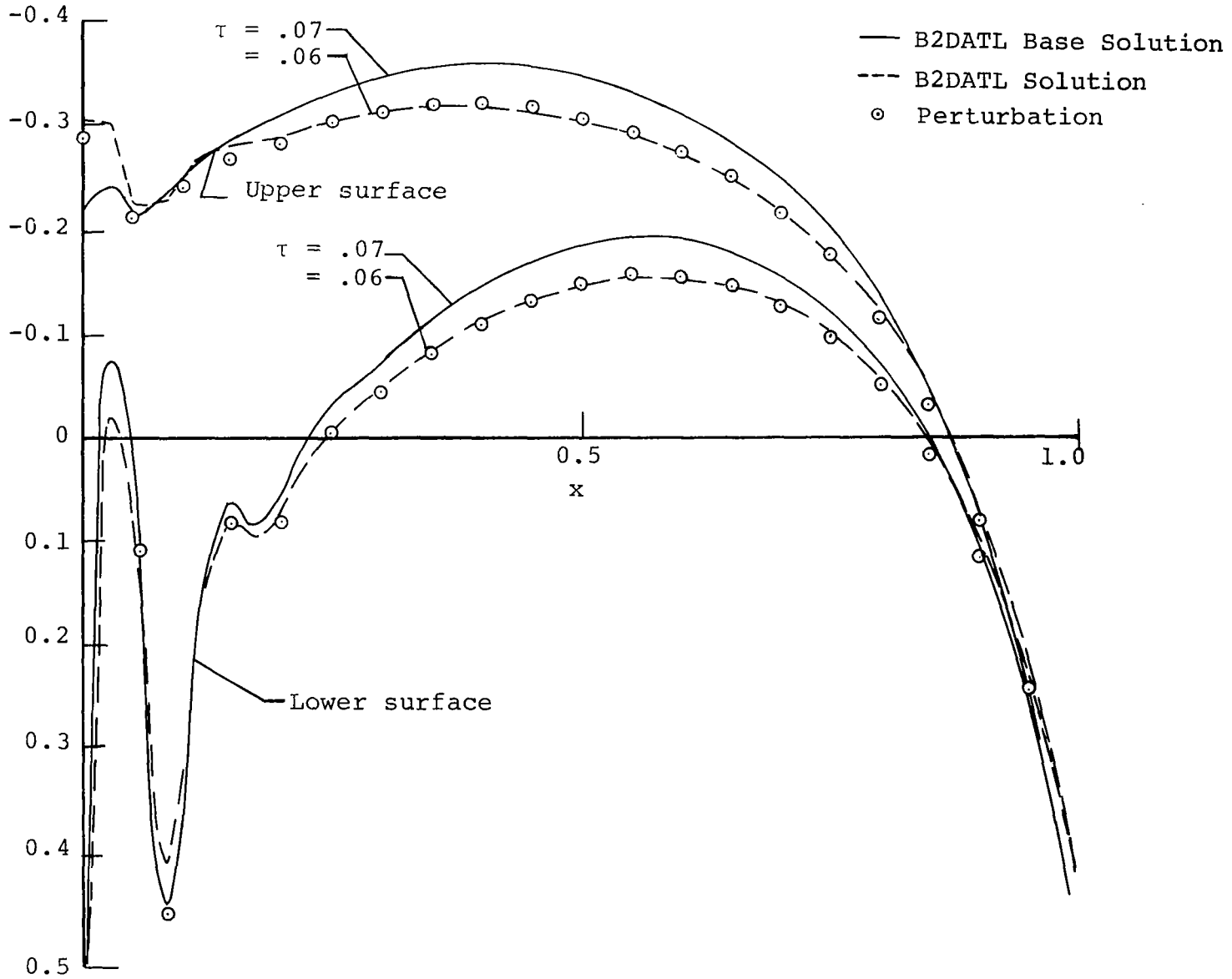

Figure 18.- Subsonic τ perturbation solutions obtained using B2DATL base solution and CASCDE perturbation code.

Ordinary perturbation solution - Obtained by differencing two nonlinear solutions given in physical coordinates x.

New perturbation solution - Obtained by differencing two nonlinear solutions after introducing strained coordinates x' such that two shock locations (and leading and trailing edges) are brought together.

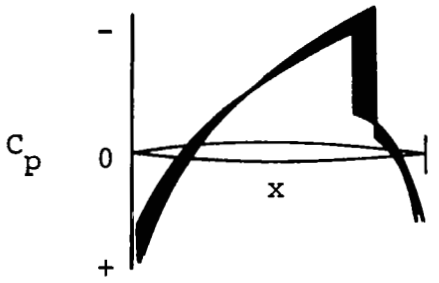

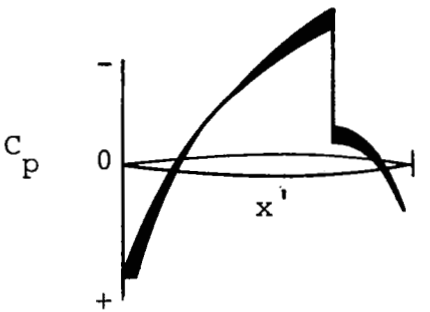

Shaded area represents perturbation solution.

Note large perturbations resulting from shock movement.

Shaded area represents perturbation solution.

Note large perturbations associated with shock movement have been removed.

Figure 19.- Perturbation shock displacement and proper definition of perturbation solution via method of strained coordinates.

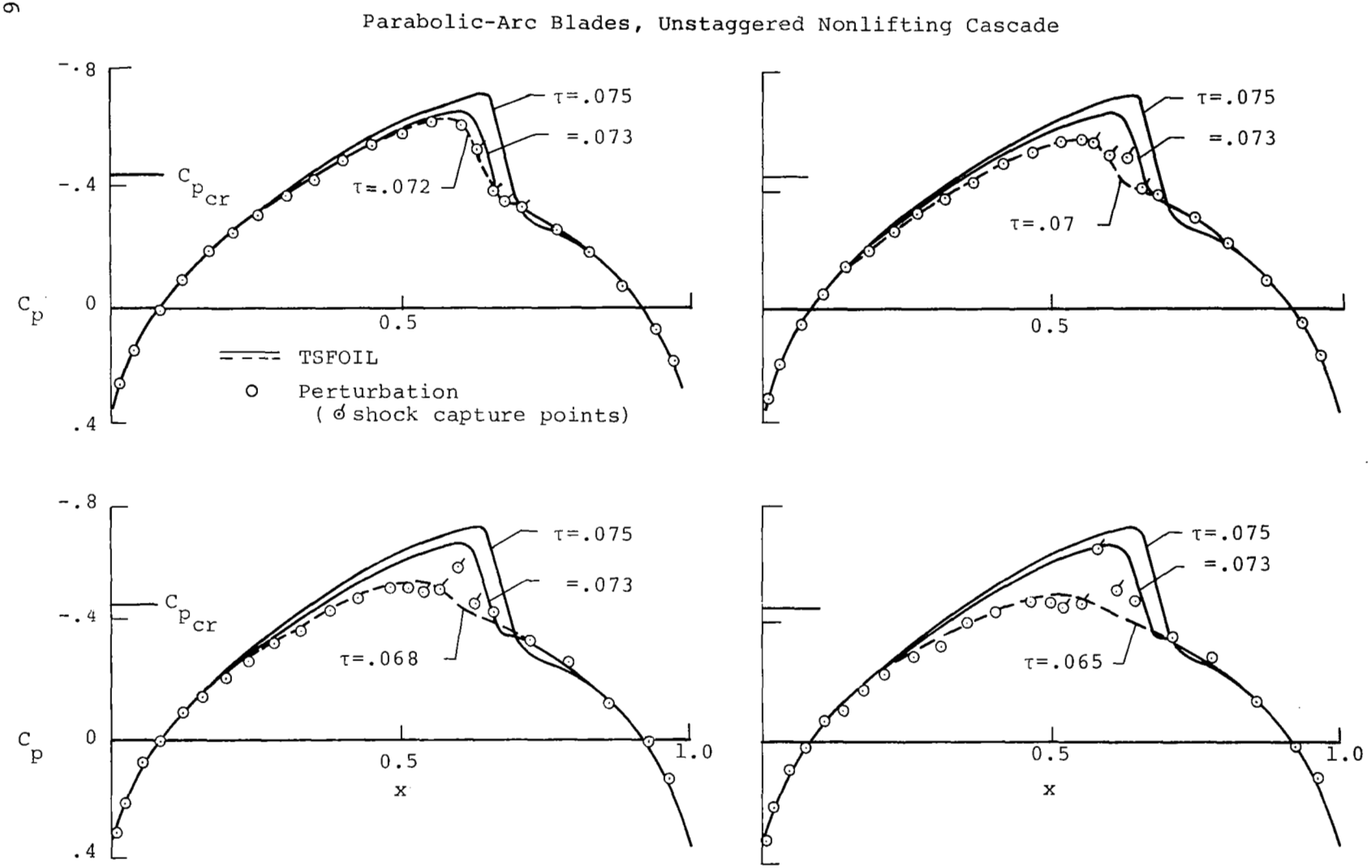

Figure 20.- Supercritical τ perturbation results with strained coordinate nonlinear differencing method using base results for τ = 0.075 and 0.073, M_1 = 0.80, H/C = 2.0.

1. Report No.	2. Government Accession No.	3. Recipient's Catalog No.
NASA CR-2941		

4. Title and Subtitle	5. Report Date
PERTURBATION SOLUTIONS FOR TRANSONIC FLOW ON THE BLADE-TO-BLADE SURFACE OF COMPRESSOR BLADE ROWS	January 1978
	6. Performing Organization Code

7. Author(s)	8. Performing Organization Report No.
Stephen S. Stahara, Denny S. Chaussee, and John R. Spreiter	NEAR TR 136
	10. Work Unit No.

9. Performing Organization Name and Address	11. Contract or Grant No.
Nielsen Engineering & Research, Inc. 510 Clyde Avenue Mountain View, California 94043	NAS3-19738
	13. Type of Report and Period Covered
12. Sponsoring Agency Name and Address	Contractor Report
National Aeronautics and Space Administration Washington, D.C. 20546	14. Sponsoring Agency Code

15. Supplementary Notes

Final report. Project Manager, William D. McNally, Fluid System Components Division, NASA Lewis Research Center, Cleveland, Ohio 44135

16. Abstract

A preliminary investigation was conducted to establish the theoretical basis of perturbation techniques with the objective of minimizing computational requirements associated with parametric studies of transonic flows in turbomachines. The theoretical analysis involved the development of perturbation methods for determining first-order changes in the flow solution due to variations of one or more geometrical or flow parameters. The formulation is primarily directed toward transonic flows on the blade-to-blade surface of a single-blade-row compressor. Two different perturbation approaches were identified and studied. Applications and results of these methods for various perturbations are presented for selected two-dimensional transonic cascade flows to illustrate the advantages and disadvantages of each technique. Additionally, it was found that, for flows with shock waves, proper account of shock displacement was crucial.

17. Key Words (Suggested by Author(s))	18. Distribution Statement
Transonic flow; Compressors; Perturbation theory; Steady flow; Blade-to-blade surface	Unclassified - unlimited STAR Category 01

19. Security Classif. (of this report)	20. Security Classif. (of this page)	21. No. of Pages	22. Price*
Unclassified	Unclassified	70	A04

* For sale by the National Technical Information Service, Springfield, Virginia 22161

NASA-Langley, 1978